Journal of Computational Neuroscience 11, 19–42, 2001

Do Neocortical Pyramidal Neurons Display Stochastic Resonance?

MICHAEL RUDOLPH AND ALAIN DESTEXHE
Unité de Neurosciences Intégratives et Computationnelles, CNRS, Bat. 33, Avenue de la Terrasse 1, 91198 Gif-sur-Yvette, France; Department of Physiology, Laval University, Québec G1K 7P4, Canada
Michael.Rudolph@iaf.cnrs-gif.fr
Alain.Destexhe@iaf.cnrs-gif.fr

Received June 22, 2000; Revised March 30, 2001; Accepted April 2, 2001

Action Editor: Dr. E. Fetz

Abstract. Neocortical pyramidal neurons in vivo are subject to an intense synaptic background activity that has a significant impact on various electrophysiological properties and dendritic integration. Using detailed biophysical models of a morphologically reconstructed neocortical pyramidal neuron, in which synaptic background activity was simulated according to recent measurements in cat parietal cortex in vivo, we show that the responsiveness of the cell to additional periodic subthreshold stimuli can be significantly enhanced through mechanisms similar to stochastic resonance. We compare several paradigms leading to stochastic resonance-like behavior, such as varying the strength or the correlation in the background activity. A new type of resonance-like behavior was obtained when the correlation was varied, in which case the responsiveness is sensitive to the statistics rather than the strength of the noise. We suggest that this type of resonance may be relevant to information processing in the cerebral cortex.

Keywords: cerebral cortex, synaptic background activity, neocortex, noise, computational models

1. Introduction

Over the last two decades, phenomena like the amplification of weak signals or the improvement of signal detection and reliability of information transfer in nonlinear dynamical systems in the presence of a certain nonzero noise level were subject of an increasing number of theoretical and experimental investigations. They became well known and are now well established under the term *stochastic resonance* (SR). Since its first appearance as a possible explanation of the periodicity of Earth's ice ages (Benzi et al., 1981; Nicolis, 1982), SR has shown to be an inherit property of many physical, chemical and biological systems. For a comprehensive review and up-to-date summary of the basic theoretical principles underlying SR, experimental verifications, and applications, we refer to Gammaitoni et al. (1998) and references therein.

Neurons provide particularly favorable conditions for displaying SR—namely, they are strongly excitable and nonlinear, and often they are subject to noisy environments. Indeed, evidence for SR was found in neurons, both theoretically (e.g., Bezrukov and Vodyanoy, 1997; Bulsara et al., 1991; Capurro et al., 1998; Chow et al., 1998; Huber et al., 1998; Lee et al., 1998; Lee and Kim, 1999; Longtin, 1993; Longtin and Chialvo, 1998; Mar et al., 1999; Mato, 1998; Neiman et al., 1999a, 1999b; Shimokawa et al., 1999; Wang et al., 1998; Wiesenfeld and Moss, 1995) and experimentally (e.g., Chialvo and Apkarian, 1993; Collins et al., 1995, 1996; Denk and Webb, 1989; Douglas et al., 1993; Ivey et al., 1998; Jaramillo and Wiesenfeld, 1998; Levin and Miller, 1996; Pei et al., 1996; Richardson et al.,

1998; Simonotto et al., 1997; Srebo and Malladi, 1999). These studies conclude that noise could play an essential role in the enhancement of signal detection and transmission, especially in sensory and peripheral nervous systems. On the other hand, due to technical difficulties, SR remains poorly characterized in the central nervous system. Recently, it was shown that the presence of noise affects the detection of distal synaptic inputs in rat hippocampal CA1 neurons in vitro (Stacey and Durand, 2000). It was proposed that SR, besides the amplification due to active channels in the dendritic tree (Cook and Johnston, 1997; Johnston et al., 1996; Magee and Johnston, 1995b; Segev and Rall, 1998; Stuart and Sakmann, 1994), could provide an alternative mechanism capable for enhancing distal synaptic input detection.

In the neocortex, each pyramidal cell is embedded in a very dense network and receives several thousands of synaptic inputs from other neurons (Cragg, 1967; DeFelipe and Fariñas, 1992; Gruner et al., 1974; Szentagothai, 1965). With a spontaneous firing rate of 5 to 20 Hz in awake animals (Evarts, 1964; Hubel, 1959; Matsumura et al., 1988; Steriade, 1978; Steriade et al., 2001), cortical cells are subject to a tremendous synaptic bombardment that leads to a highly fluctuating intracellular activity (e.g., Azouz and Gray, 1999; Contreras et al., 1996; Destexhe and Paré, 1999; Hô and Destexhe, 2000; Lampl et al., 1999; Matsumura et al., 1988; Nowak et al., 1997; Paré et al., 1998). In this article, we investigate whether this type of fluctuating activity can lead to SR in neocortical pyramidal neurons. We used computational models of morphologically reconstructed neurons in which synaptic background activity was simulated according to recent measurements in cat parietal cortex in vivo (Destexhe and Paré, 1999; Paré et al., 1998). This approach departs from classic SR paradigms because here the "noise" (background activity) is not external but is generated by the cortex itself. We discuss its implications and predictions for information processing by cortical neurons.

Part of these results have appeared in a conference abstract (Rudolph and Destexhe, 2000).

2. Methods

2.1. Model Settings

Computational simulations were performed using a morphologically reconstructed neocortical pyramidal layer VI neuron of a cat (Fig. 1A) obtained from a previous study (Contreras et al., 1997). The dendritic surface was corrected for spines under the assumption that about 45% of the dendritic membrane area are represented by spines (DeFelipe and Fariñas, 1992).

The passive model parameters (Table 1), which were kept constant in all simulations, were estimated by matching the model to passive responses obtained intracellularly after application of TTX and synaptic blockers (Destexhe and Paré, 1999).

For most of the models, three types of active ionic currents (fast sodium current I_{Na}, delayed-rectifier potassium current $I_{\mathrm{K\,d}}$ and V_m-dependent potassium current I_{M}) were simulated by inserting voltage-dependent conductances, described by Hodgkin-Huxley type models, in the soma, dendrites and the axon (Table 2). The kinetics of the currents were taken from a model of hippocampal pyramidal cells (Traub and Miles, 1991) in which inactivation was shifted 10 mV towards hyperpolarized values in order to match voltage-clamp data of cortical pyramidal cells (Huguenard et al., 1988). To discuss the impact of membrane excitability, the peak conductances of all ion channels were altered by a common multiplicative factor a_{ic}. Here, three cases were investigated: a low excitabi- lity ($a_{\mathrm{ic}} = 0.4$, corresponding to the lower border of the experimental observed range), a medium ("mid") excitability ($a_{\mathrm{ic}} = 0.7$, corresponding to values found experimentally in adult hippocampal pyramidal neurons) (see Magee and Johnston, 1995a), and a high excitability ($a_{\mathrm{ic}} = 1$). The robustness of the results was tested by using different sets of voltage-dependent conductances, which included a Ca^{2+}-dependent potassium current (C-current) $I_{\mathrm{K\,Ca}}$ (kinetics in Yamada et al., 1989; constant dendritic conductance density of 1 mS cm^{-2}), a high-threshold Ca^{2+}-current (L-current)

Table 1. General passive parameter settings (reversal potential E_{rev}, axial resistivity R_{axial}, leak conductances g_{leak}, and capacitances C for the axon, soma and dendrites) used in the models.

$g_{\mathrm{leak\,axon}} = 0.02$ S cm^{-2}	$C_{\mathrm{axon}} = 0.04\ \mu$F cm^{-2}	$E_{\mathrm{rev}} = -80$ mV
$g_{\mathrm{leak\,soma}} = 4.52 \cdot 10^{-5}$ S cm^{-2}	$C_{\mathrm{soma}} = 1.449\ \mu$F cm^{-2}	$R_{\mathrm{axial}} = 250\ \Omega$cm
$g_{\mathrm{leak\,dend}} = 6.5495 \cdot 10^{-5}$ S cm^{-2}	$C_{\mathrm{dend}} = 1\ \mu$F cm^{-2}	

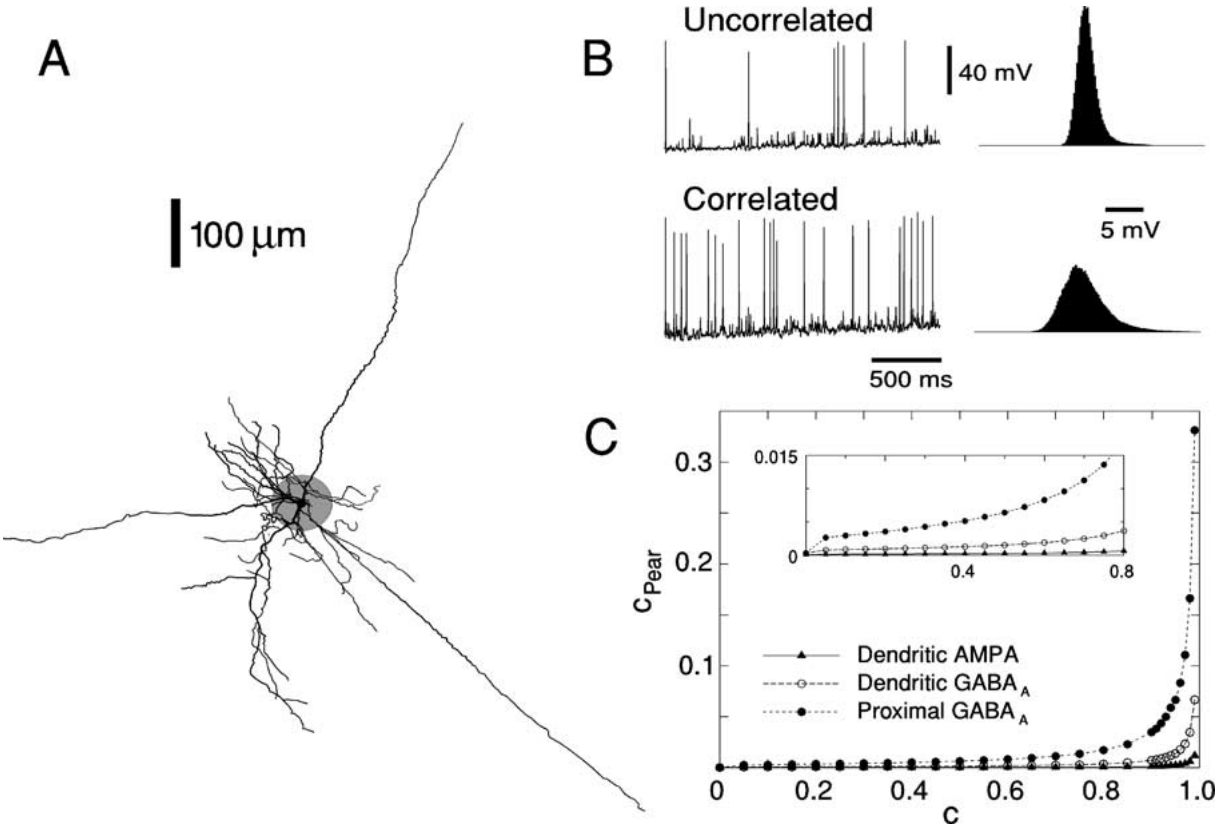

Figure 1. Synaptic background activity leads to membrane potential fluctuations and spontaneous firing activity. **A:** Morphologically reconstructed neocortical pyramidal layer VI neuron of a cat incorporated in the models. The shaded area indicates the proximal region including all dendritic branches within a radius of 40 μm from the soma. Inside that region there were no excitatory synapses, whereas inhibitory synapses were spread over the whole dendritic tree. **B:** V_m fluctuations (left) due to synaptic background activity. Poisson-like distributed random inputs without correlation led to small-amplitude fluctuations, whereas the amplitude and number of spontaneously elicited spikes was much higher when correlation between individual synaptic release events was introduced. In all cases, synaptic background activity led to a nearly Gaussian-like amplitude distribution of V_m fluctuations (right). **C:** Relation between Pearson's correlation coefficient c_{Pear} of the synaptic release events and the parameter c used in the distributed generator algorithm for various types of synapses.

$I_{\mathrm{Ca\,L}}$ (kinetics in McCormick and Huguenard, 1992; conductance density of 3 mS cm^{-2} and 1.5 mS cm^{-2} for proximal and distal dendrites, respectively), and a persistent sodium current $I_{\mathrm{Na\,P}}$ (kinetics in French et al., 1990; Huguenard and McCormick, 1992; McCormick and Huguenard, 1992; constant dendritic conductance density of 0.1 mS cm^{-2}), as well as a model with different kinetics for I_{Na}, $I_{\mathrm{K\,d}}$ and an A-type potassium current $I_{\mathrm{K\,A}}$ (models from Migliore et al., 1999).

Synaptic currents were incorporated by using two-state kinetic models (Destexhe et al., 1998) of glutamate α-amino-3-hydroxy-5-methyl-4-isoxazole-propionic acid (AMPA) and γ-aminobutyric acid type-A (GABA$_A$) receptors (Table 3). No metabotropic receptors were included. The densities of synapses in different regions of the cell were estimated from morphological studies in neocortical pyramidal neurons (DeFelipe and Fariñas, 1992; Larkman, 1991; White, 1989), leading to a total number of 16,563 glutamatergic and 3,376 GABA$_A$ergic synapses (2,818 in dendritic and 558 in proximal region) for the layer VI cell under consideration. To perform the simulations in a time-efficient manner, an accelerating algorithm (Lytton, 1996) was used to handle the synaptic activation.

Synaptic background activity was simulated by the firing of inhibitory and excitatory synapses. Appropriate release conditions, which were estimated based on recent data from intracellular recordings of pyramidal neurons before and after application of TTX (Destexhe and Paré 1999; Paré et al., 1998), correspond to all presynaptic terminals releasing randomly

Table 2. Parameter settings for voltage-dependent ionic currents used in the models (reversal potential E, conductance densities $\bar{g}$). The factor a_{ic} was changed to rescale ion channel densities to obtain models with various membrane excitability (see Section 2, Methods).

Fast sodium channels I_{Na}	Delayed-rectifier potassium channels $I_{\text{K d}}$	V_m-Dependent potassium channels I_{M}
$E_{\text{Na}} = 50$ mV	$E_{\text{K}} = -90$ mV	
$\bar{g}_{\text{Na axon}} = a_{\text{ic}} \cdot 516$ mS cm^{-2}	$\bar{g}_{\text{Kd axon}} = a_{\text{ic}} \cdot 100$ mS cm^{-2}	
$\bar{g}_{\text{Na soma}} = a_{\text{ic}} \cdot 51.6$ mS cm^{-2}	$\bar{g}_{\text{Kd soma}} = a_{\text{ic}} \cdot 10$ mS cm^{-2}	$\bar{g}_{\text{M soma}} = a_{\text{ic}} \cdot 0.5$ mS cm^{-2}
$\bar{g}_{\text{Na dend}} = a_{\text{ic}} \cdot 74.8$ mS cm^{-2}	$\bar{g}_{\text{Kd dend}} = a_{\text{ic}} \cdot 14.5$ mS cm^{-2}	$\bar{g}_{\text{M dend}} = a_{\text{ic}} \cdot 0.725$ mS cm^{-2}

Table 3. Parameter settings for synaptic currents used for simulating background activity as well as additional stimulation. The common factor a_{sc} was introduced to adjust synaptic quantal conductances (see Section 2, Methods). For details about the kinetic models used, we refer to Destexhe et al. (1998).

GABA$_A$ synapses	AMPA synapses	Stimulating AMPA synapses
$\alpha_{\text{mGABAa}} = 5$ ms^{-1} mM^{-1}	$\alpha_{\text{mAMPA}} = 1.1$ ms^{-1} mM^{-1}	$\alpha_{\text{AMPA stim}} = 1.1$ms^{-1} mM^{-1}
$\beta_{\text{mGABAa}} = 0.1$ ms^{-1}	$\beta_{\text{mAMPA}} = 0.67$ ms^{-1}	$\beta_{\text{AMPA stim}} = 0.19$ ms^{-1}
$C_{max\,\text{mGABAa}} = 1$ mM	$C_{max\,\text{mAMPA}} = 1$ mM	$C_{max\,\text{AMPA stim}} = 1$ mM
$C_{dur\,\text{mGABAa}} = 1$ ms	$C_{dur\,\text{mAMPA}} = 1$ ms	$C_{dur\,\text{AMPA stim}} = 1$ ms
$E_{rev\,\text{mGABAa}} = -75$ mV	$E_{rev\,\text{mAMPA}} = 0$ mV	$R_{rev\,\text{AMPA stim}} = 0$ mV
		$E_{pre\,thres\,\text{AMPA stim}} = 0$ mV
		$T_{dead\,\text{AMPA stim}} = 1$ ms
$g_{\text{GABAa dend}} = a_{\text{sc}} \cdot 869.4$ pS	$g_{\text{AMPA dend}} = a_{\text{sc}} \cdot 1738.8$ pS	$g_{\text{AMPA stim}} = 0.1$ mS cm^{-2}
$g_{\text{GABAa prox}} = a_{\text{sc}} \cdot 600$ pS		
$N_{\text{GABAa dend}} = 2818$	$N_{\text{AMPA dend}} = 16563$	$N_{\text{AMPA stim}} = 197$
$N_{\text{GABAa prox}} = 558$		

according to a Poisson-like process with average rates of $\nu_{\text{inh}} = 5.5$ Hz for GABA$_A$ synapses and $\nu_{\text{exc}} = 1.0$ Hz for AMPA synapses. In addition, the distributed nature of the synaptic release allowed to modify the statistics of the background activity by introducing a redundancy in the Poisson-distributed random numbers assigned to the presynaptic compartments: At each time step, $N_0 = N + \sqrt{c}\ (1 - N)$ Poisson-distributed random synaptic events were generated and randomly redistributed among N synaptic channels. For $N_0 < N$ this leads to a simultaneous ("correlated") release of some of the N synapses, whereas each individual synapse still releases randomly according to the same Poisson distribution. The average correlation for every pair of synapses was the same irrespective of their location within the dendritic tree. The procedure allows to control the correlation of the background independently, by changing N_0, without affecting the average release frequency at each synapse and thus without changing the overall conductance due to background activity. Details of this distributed generator algorithm can be found in Destexhe and Paré (1999). In what follows, the correlation parameter c rather than the Pearson's correlation coefficient is used to label various statistics because it is directly related to the generating algorithm. Independent generators were chosen for proximal and dendritic GABA$_A$ as well as AMPA synapses, leading to different relations between c and c_{Pear}, as shown in Fig. 1C.

To investigate the effect of additionally applied subthreshold periodic stimulation, a supplementary set of AMPA-mediated synapses (equivalent kinetic model, total of 197 synapses in dendritic region) was introduced into the model (see Table 3). The conductance density of these synapses, which represented only a small fraction of the total AMPA conductance available in the dendrites, was uniform in dendrites and kept fixed through all simulations. The stimulation was obtained by firing of all of these additional synapses at the same time with a constant period of $T_{\text{stim}} = 100$ ms,

which was chosen as a compromise between the desired high statistics, limited by computationally extensive simulations, and the necessity of independent stimuli. Successive stimuli can be considered as independent because T_{stim} is large compared to the typical duration of the responses (post-stimulus-time histograms are of the order of 15 to 20 ms) (see Hô and Destexhe, 2000).

The cellular geometry was incorporated into the NEURON simulation environment (Hines and Carnevale, 1997), which was used for all simulations. In the case of background activity and additional stimulation, 60 s neuron activity were simulated for each parameter set, leading to a total of 600 stimulation events. For simulations with background only, the simulation time was fixed to 30 s. In all cases a time resolution of 0.1 ms was used. Spike train and the membrane voltage V_m were recorded at the soma during the whole simulation.

All computations were performed using a DELL Dimension XPS T600 (Dell Computer Corporation, Round Rock TX, USA) running under the LINUX operating system.

2.2. *Data Analysis and Measures of Response Coherence*

Voltage records with a time resolution of 0.1 ms and records of spike release events at the soma in conjunction with recordings of individual synaptic firing events for each model parameter set constitute the data basis for the presented investigations. Besides a standard statistical analysis of the voltage records and spike trains, inter-spike-interval (ISI) and joint-interval (JI) histograms with binsizes between 2 and 15 ms, post-stimulus-time histograms (PSTH) with a temporal resolution of 0.5 ms and the (average and cumulative) voltage after stimulation with a resolution of 0.1 ms were obtained. In addition, for each parameter set power spectral densities (PSDs) were calculated for the voltage and spike trains using a complex discrete fast Fourier transform (based on Press et al., 1993) with a sampling frequency of 10,000 Hz, with $2^{19} = 524{,}288$ data points for the 60 s noise plus stimulation, and 2^{18} data points for the 30 s noise-only simulations. This led to a frequency resolution of 0.038 Hz in the case of noise-only and 0.019 Hz for noise-plus-stimulus simulations.

Various ways were used to characterize and quantify the response of the neuron to the periodic stimulus (for a detailed overview we refer to Gammaitoni et al., 1998).

2.2.1. Power Spectral Analysis. The most common way to characterize SR in the response of dynamical systems is in terms of the signal-to-noise ratio (SNR) following from the analysis of PSDs. A variety of mathematical implementations of this ratio, which simply measures the ratio of the "strength" of the peak at some typical frequency ν_0 (usually the frequency of the periodic stimulus), and the strength of the background at this frequency) exists in the literature (e.g., Fauve and Heslot, 1993; Lee and Kim, 1999; Wiesenfeld and Moss, 1995; Zhou and Moss, 1990), each leading to similar results. In the present study we have made use of the following definition:

$$\text{SNR} = 10 \cdot \log_{10} \left[N(\nu_0)^{-1} \int_{\nu_0 - \Delta\nu}^{\nu_0 + \Delta\nu} \mathrm{d}\nu \, P(\nu) \right], \quad (1)$$

where $P(\nu)$ and $N(\nu)$ denote the PSDs at frequency ν in the spike train power spectra obtained from signal with background noise and noise-only simulations, respectively. Due to the finite time resolution in our simulations, the ideal limit $\Delta\nu \to 0$ was replaced by the finite value $2 \cdot \Delta\nu = 0.1$ Hz. Note that this definition of the SNR does not necessarily lead to a zero value when there is no signal peak above the background in the noise-plus-stimulus power spectrum.

Because a subthreshold periodic stimulation leads to periodic EPSPs, which show up as peaks at appropriate frequencies in the V_m power spectra, another way to characterize the cell's response to a stimulation is given by the "strength" of the corresponding EPSPs, deduced from the voltage PSDs. To that end, a SNR according to (1) was defined for the membrane voltage, and analyzed as a function of the background properties.

2.2.2. ISI Distribution. As it was shown in computational investigations of simple neuron models (Longtin, 1993; Wiesenfeld and Moss, 1995) as well as in experimental studies (e.g., Douglas et al., 1993; Ivey et al., 1998), in the presence of a periodic force the neural system responds with spike trains whose ISI histograms contain a series of peaks centered at multiples of some period T_0, which in many cases equals the period of this force T_{stim}. The height of the peaks usually decreases exponentially with increasing order but also depends on the noise and stimulus properties. Detailed studies of bistable systems and simple models of excitable membranes (see Longtin, 1993) revealed that the height of peaks with fixed order goes through a maximum as a function of noise intensity, and thus can be viewed as a

measure of the coherence or synchronization between the periodic forcing and the particular behavior of the system leading to the genesis of spikes. In the present study we investigated if the results deduced from simple neuron models also apply in more realistic models. As a measure of the "strength" of the peaks in the ISI histogram we used the ISI density, defined by

$$\mathrm{ISID}_i = \frac{N_{\mathrm{ISI}i}}{N_{\mathrm{total}} \times T_{\mathrm{bin}}} \sim \begin{array}{l}\text{relative height of peak} \\ \text{in ISI histogram}\end{array}. \quad (2)$$

Here, $N_{\mathrm{ISI}i}$ denotes the number of ISIs with length $T_{\mathrm{ISI}i} = i \cdot T_{\mathrm{stim}}$, where T_{stim} is the period of the stimulus and i is the order of the peak in the ISI histogram, and N_{total} denotes the total number of ISIs. The $N_{\mathrm{ISI}i}$ used in the analysis were obtained from ISI histograms with binsizes T_{bin} of 5 and 15 ms for periods of T_{ISI1}, T_{ISI2} and T_{ISI3}, respectively.

2.2.3. Coherence Between Output and Stimulus. Another measure describing the response of the system in terms of the statistical properties of spike trains is given by the coherence between the output and the stimulus (Chialvo and Apkarian, 1993):

$$\mathrm{COS}_i = \frac{N_{\mathrm{ISI}i}}{N_{\mathrm{total}}}, \quad (3)$$

where N_{total} denotes the total number of spikes fired in a fixed time interval T after the stimulation.

In the present study, the time interval T was taken to be the total length of the corresponding simulations. The number of ISIs, $N_{\mathrm{ISI}i}$, were obtained from the ISI histograms with a binsize of 15 ms for periods of T_{ISI1}, T_{ISI2} and T_{ISI3}, respectively. Smaller binsizes led to qualitatively equivalent results.

2.2.4. Probability for Evoking Spikes. The last measure we will use in quantifying the response of the neuron is the probability of spikes specifically evoked by the stimulus, defined by

$$P_{\mathrm{spikes}} = \frac{N_{\mathrm{spikes}}}{N_{\mathrm{total}}}, \quad (4)$$

where N_{spikes} denotes the number of evoked spikes in a fixed time interval after the stimulus, cumulated for all stimuli, and N_{total} is the total number of evoked spikes. This measure is similar to the time-integrated PSTH (Hô and Destexhe, 2000). A SNR corresponding to P_{spikes} can be introduced by using the standard deviation σ_V, obtained from voltage records of simulations with noise and stimulus, as a measure for the background activity:

$$\mathrm{SNR}^* = \frac{P_{\mathrm{spikes}}}{\sigma_V}. \quad (5)$$

For the analysis presented in this article, the number of evoked spikes in time intervals of length 10 ms as well as 20 ms after each stimulus were cumulated to yield N_{spikes}.

To capture the resonance behavior, unless otherwise stated, COS and ISId data as well as the SNR deduced from spike PSDs were fitted using functions of the form $P_2(x)\exp(-(x-a)^2/b^2)$, $\frac{P_2(x)}{x^2}\exp(a/x)$ or $\frac{P_2(x)}{x^2}\exp(-ax)$, where $P_2(x)$ denotes a polynomial of second order. Due to an expected different functional behavior of the SNR* measure (see Section 3, Results), corresponding data were fitted by an exponential $a\,\mathrm{e}^{-bx}$. The SNR deduced from voltage power spectra was fitted by a quadratic function.

3. Results

We begin by outlining some general properties of the model and motivate its investigation in the framework of SR-like phenomena by raising the question of how the background activity affects the coherence between the response of the cell and an additionally applied periodic stimulus. In a first part, we show how the strength of the synaptic background affects the response coherence. This was done by changing either the quantal conductances of the synapses subject to the background activity (conductance study) or the release frequency of the excitatory background (frequency study). In a second part, we investigated the impact of the correlation in the background activity (correlation study) on the response of the cell.

As described in Section 2, Methods, we simulated a model of synaptic background activity that was introduced previously (Destexhe and Paré, 1999) and that was based on intracellular recordings in cat parietal neurons in vivo (Paré et al., 1998). Synaptic background activity was simulated by high-frequency release conditions at excitatory and inhibitory synapses, which were matched to experimental measurements. These conditions could simulate the typical electrophysiological parameters measured intracellularly in

vivo (Destexhe and Paré, 1999; Paré et al., 1998), such as a depolarized V_m around -65 mV, an about five-fold lower input resistance, high-frequency V_m fluctuations with an approximately symmetric (Gaussian) amplitude distribution ($\sigma_V \sim 4$ mV), and spontaneous firing activity between 5 and 20 Hz (see Fig. 1B). To reproduce all properties, it was necessary to introduce a weak correlation between release events, labeled by the parameter c in the distributed generator algorithm (see Section 2, Methods). The relation between this parameter and Pearson's correlation coefficient c_{Pear} is given in Fig. 1C. The weak correlation was in agreement with the level of correlation measured between pairs of cortical neurons in awake monkeys (Zohary et al., 1994).

3.1. Conductance Study: The Impact of Background Conductance Density

We first investigated the model in the framework of classical SR by changing the strength of the synaptic background. To that end, we introduced a common multiplicative factor a_{sc}, which was applied to the value of excitatory and inhibitory conductances. Here and in what follows the term *strength* refers to the time-averaged impact on the cell. a_{sc} was altered in the range $0.50 \leq a_{\text{sc}} \leq 1.95$ with a stepsize of $\Delta a_{\text{sc}} = 0.05$. To investigate how additional correlation in the synaptic background affects the behavior of the cell, two sets of simulations with $c = 0.0$ and $c = 0.7$ were performed. All simulations were done by using ion channel densities corresponding to medium excitability (see Section 2, Methods).

A change of a_{sc} in the given range has had two major effects on V_m. First, increasing conductances led to a slightly increasing depolarization of the membrane between -67 mV for $a_{\text{sc}} = 0.5$ and -64 mV for $a_{\text{sc}} = 1.95$ for both correlation values (see Fig. 2A). Similar, the amplitude of V_m fluctuations, measured by the standard deviation σ_V, showed a smooth increase between $1 \text{ mV} \leq \sigma_V \leq 3$ mV for $c = 0.0$ and $2 \text{ mV} \leq \sigma_V \leq 4$ mV for $c = 0.7$ (Fig. 2B). Whereas the quantitative and qualitative behavior of the average V_m as a function of a_{sc} was the same for both correlation settings, we observed higher-fluctuation amplitudes for $c = 0.7$, reflecting the fact that a simultaneous firing of single synapses has a much stronger impact on V_m than their independent activation. However, it is remarkable that only the height of the fluctuations was affected by the correlation but not the fluctuation range. In both cases, the effective change in σ_V was about 2 mV over the chosen a_{sc} parameter range. Moreover, for high synaptic conductances the average V_m as well as σ_V did not further increase but instead showed a saturation behavior by converging toward fixed values. Additional simulations done for even higher a_{sc} (data not shown) supported this observation. This result could be explained by a very stable balance between inhibitory and excitatory inputs, which was not affected by the present simulation settings. However, the frequency study (see below), which directly altered this balance by modifying the excitatory firing rate only, revealed a qualitatively similar behavior for the corresponding quantities. Finally, the additional periodic stimulation has had only a minor influence on σ_V, which decreased further for higher correlation.

In both cases, the number of observed spikes was low. For $c = 0.0$ practically no spikes were evoked in the noise-only simulations, even for high conductances, indicating that the background-induced V_m fluctuations were too small for spontaneously eliciting spikes. Also the combined effect of background- and stimulation-induced V_m depolarizations only sporadically led to a crossing of the firing threshold, manifesting in a spike rate of less than 0.5 Hz for higher a_{sc}. Due to an overall higher σ_V, this situation changed for $c = 0.7$. Whereas here the cell remained subthreshold for lower a_{sc}, at higher values the release rate stabilized between 7 and 8 Hz.

The effects of the additional stimulation induced a slight periodic depolarization, which led to clear peaks in the corresponding power spectra at multiples of the stimulation frequency of 10 Hz (Fig. 2E). Because of a higher number of evoked spikes in coherence with the stimulation for increasing conductances, the height of the peaks in the spectra also increases with a_{sc}. The spectral noise follows a similar behavior due to the higher fluctuation amplitudes for higher a_{sc}. In all PSDs, peaks at the signal frequency and multiples of it are higher for $c = 0.0$, whereas the spectral noise is lower due to the smaller σ_V caused by the synaptic background.

The evoking of spikes and membrane depolarization in coherence with the periodic stimulus reflect in peaks right after the stimulus in the corresponding PSTHs and average V_m after stimuli (Fig. 2C). The height of these peaks, which measure the "amplitude" of this coherent response, becomes larger for higher background strength. However, an effect of correlation

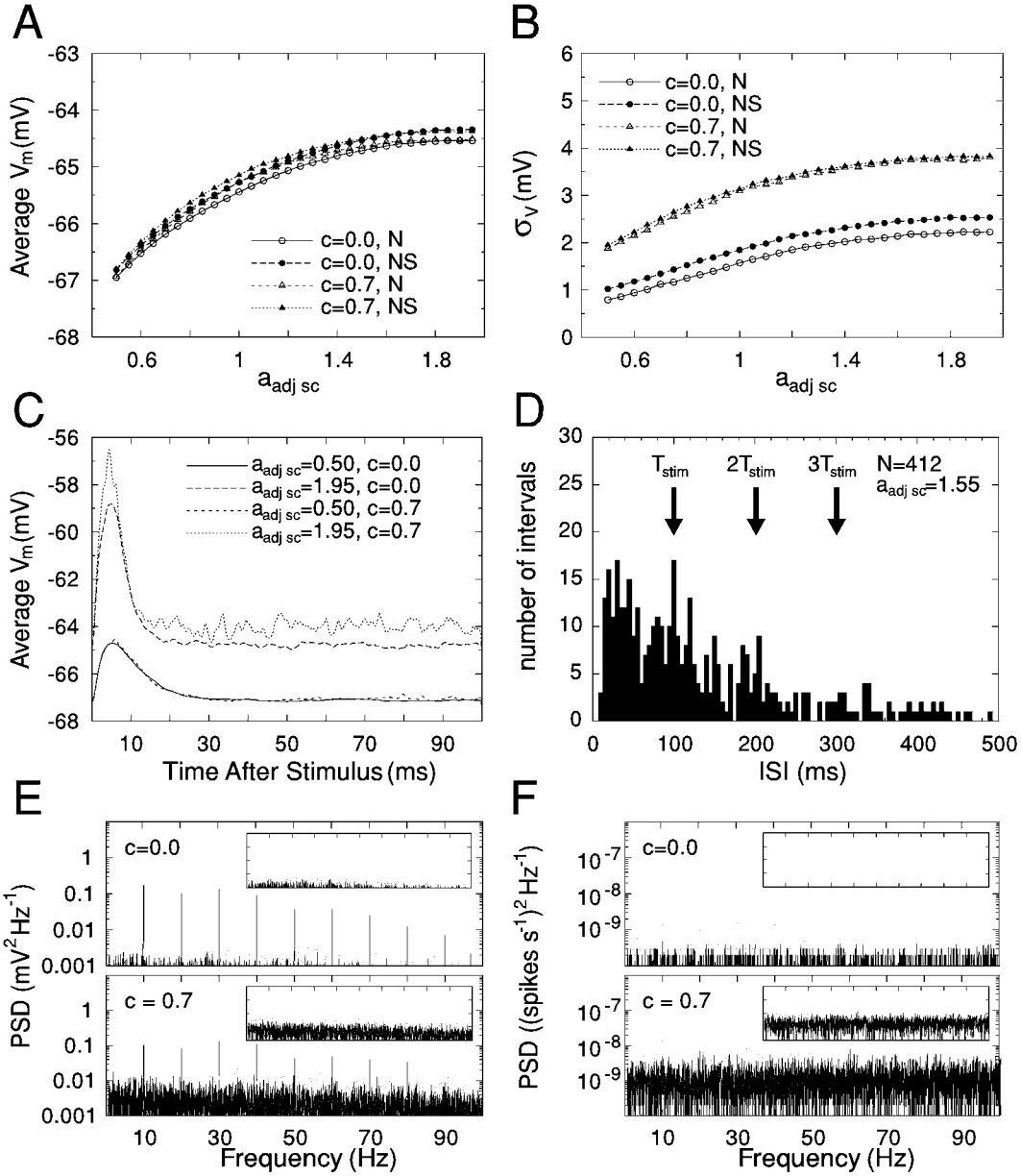

Figure 2. Behavior of the model following covariations in the quantal conductances of excitatory and inhibitory inputs. **A:** Impact of quantal synaptic conductance changes on the average V_m obtained from recordings that were cleared for spikes. Depicted are the results for simulations with noise-only (N) and noise-plus-stimulus (NS) for both correlation settings. **B:** The behavior of the standard deviation σ_V quantifying V_m fluctuations as a function of a_{sc} for simulations with background noise-only as well as noise-plus-stimulus for both correlation values. **C:** Average V_m after stimulus for two conductance settings. The evoking of spikes in coherence with the stimulus reflects in the peak right after the stimulus. **D:** Representative ISI histogram obtained from noise-plus-stimulus simulations for $a_{sc} = 1.55$ and $c = 0.7$. The distribution shows indication for peaks at multiples of the stimulation period $T_{stim} = 100$ ms but also contains a very strong background expected for Poisson-like processes. **E** and **F:** Representative PSDs of voltage records (E) and spike trains (F) obtained from noise-plus-stimulus simulations for both correlation values and $a_{sc} = 1.50$. The plots show clear peaks at multiples of the signal frequency of 10 Hz. PSDs calculated from the corresponding noise-only simulations are depicted as inlets. Channel densities corresponding to medium excitability were used in all cases.

on the responsiveness for fixed conductances is visible only for higher a_{sc}.

Due to the low number of spikes, no statistically meaningful ISI distribution or PSDs of spike trains could be derived for $c = 0.0$. A representative ISI histogram for $c = 0.7$ is depicted in Fig. 2D. It shows indications for peaks at multiples of the stimulation period of $T_{stim} = 100$ ms, in accordance with results obtained from investigations of bistable systems mentioned above. However, these peaks are partially blot out by a background expected for spike trains of Poisson-like processes. For high a_{sc} the ISI histograms take the shape of an ideal Poisson-distributed spike train with an absolute refractory period drawn from a Gaussian distribution, whereas for low quantal conductances the statistics prevented a reliable statement. Similarly, for lower amplitudes of the background it was not possible to calculate spike train PSDs. For higher a_{sc} the obtained power spectra (see Fig. 2F) show peaks at multiples of the signal frequency, whose height undergoes a maximum as a function of a_{sc}. As in the case of voltage records, the spectral noise increases with increasing conductance, and for fixed a_{sc} the noise was higher for $c = 0.7$. All measures of response coherence introduced above (see Section 2, Methods) were applied. The corresponding results for $c = 0.7$ are depicted in Figs. 3 and 4. The SR-like behavior indicated by the ISI histograms is best seen when the COS measure is depicted as a function of the noise level. For the latter we used both, a_{sc} labeling the background strength, as well as σ_V labeling the internal noise level. However, only the COS values deduced from the strongest peak in the ISI histograms (at an ISI of length T_{stim}) increase and slightly decrease for increasing background amplitude, whereas the coherence obtained from second- or higher-order peaks (data not shown) only gets stronger over the simulated conductance range. Moreover, the ISI density measure shows high fluctuations and does not allow an interpretation of the results, especially for higher-order ISI peaks. This can be traced back to the fact that the ISID was obtained from histograms with a binsize of only 5 ms, whereas the calculation of COS is based on ISI histograms with a binsize of 15 ms. But as we will see in the forthcoming frequency study and correlation study, these differences will disappear.

Additional simulations were performed up to $a_{sc} = 3.0$ to see if a significant decrease in the COS and ISID measures could be achieved (data not shown). However, due to the saturation of σ_V the effects were only marginal. In contrast, at very high conductances we obtained a slight decrease in σ_V, which indicates the limit of the present computational model.

Qualitatively different from the behavior of the COS and ISID measures is that of SNR* (Fig. 3C). Here, a sharp increase is followed by a slight exponential decrease. This can be explained by the fact that evoking of the first spikes is most likely when the combined effects of stimulation caused V_m depolarization and V_m fluctuations due to the background lead to a crossing of the firing threshold. Thus, naturally the strongest coherence between the stimulus and the spike following that stimulus event occurs for low background strength, showing up in a rapid increase of P_{spikes} and the related SNR*. For even higher background amplitudes, spikes are evoked with increasing probability in the whole time interval between two stimuli, which leads to the observed decrease of the SNR*. This way the SNR* can be viewed as an indicator for the particular background amplitude at which the system starts to respond in coherence with the external stimulus. This was the case for $c = 0.7$ at $a_{sc} \sim 0.5$ and $\sigma_V \sim 1.7$ mV.

The SNR deduced from the PSDs of the recorded spike trains shows only an slight increase toward a fixed value (Fig. 4A), which was kept nearly unaffected for even higher a_{sc} settings (data not shown). Comparing with the COS and ISID measures, the SNR graphs seem to be shifted towards smaller values of a_{sc} and σ_V. Therefore, here the maximum SNR is reached for lower background amplitudes.

We also calculated the SNR based on the voltage PSDs. Because of the peaks in the spectra caused by the periodic membrane depolarization we cannot expect to find a resonance structure. However, the behavior we observed is quite remarkable. Over the simulated parameter range, the SNR stayed nearly constant (Fig. 4B). This suggests that an increase in the background amplitude did not affect the response of the cell with respect to V_m changes due to additional stimulation, which stands in contrast to the expectation that the latter should be blurred or "smeared out" by a higher σ_V.

3.2. *Frequency Study: The Impact of Excitatory Background Firing Rates*

Another way to change the strength of the background is given by a modification of the synaptic release frequencies. However, in contrast to the previous case, in this frequency study we altered only

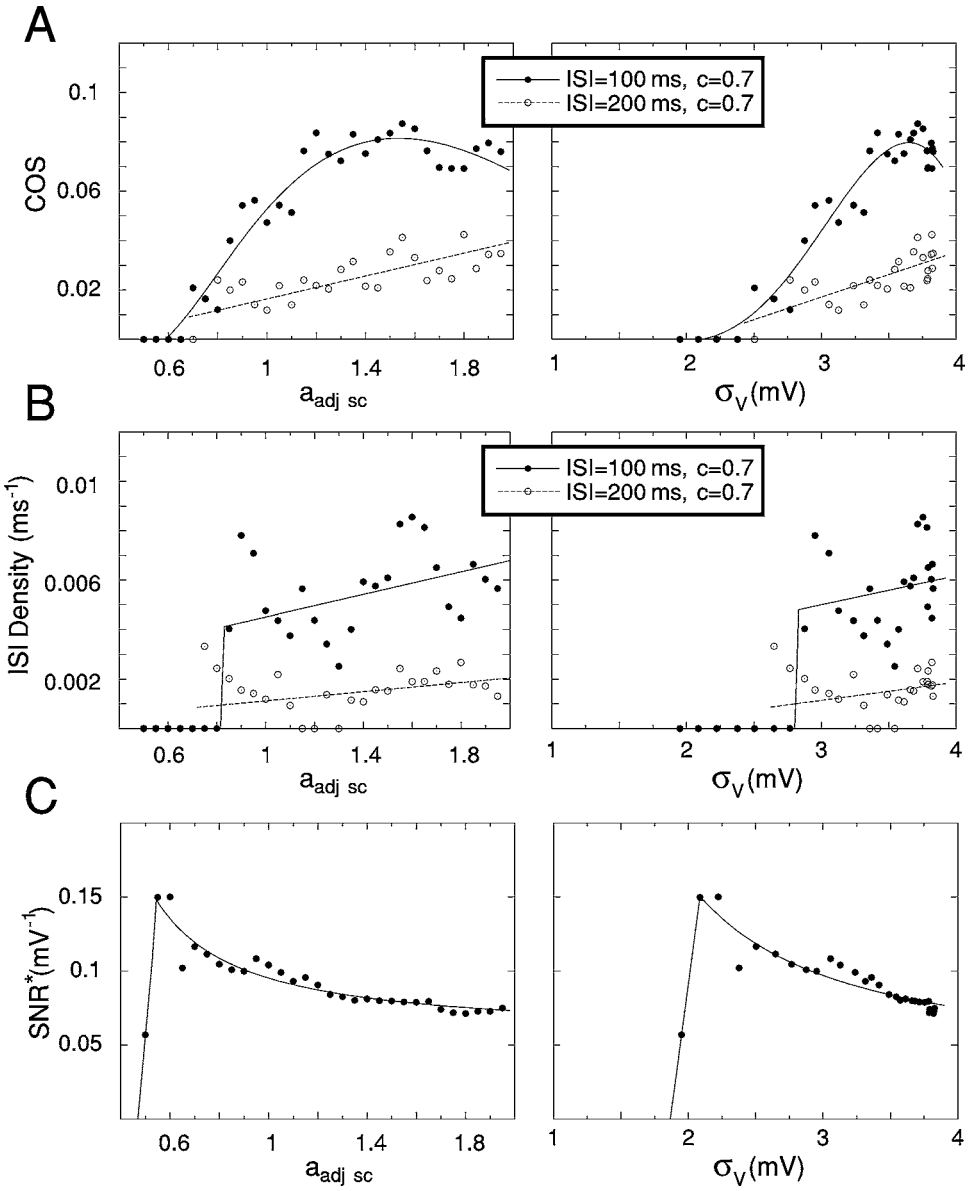

Figure 3. Classical stochastic resonance in the neuron model with changing quantal synaptic conductances. Model with medium excitability and $c = 0.7$. The left plots show the coherence measures as a function of the background amplitude labeled by a_{sc}. The right plots depict the corresponding resonance measures as a function of the voltage fluctuations σ_V resulting from background and stimulus inputs. **A:** Coherence between output and stimulus obtained from the first and second peak at 100 ms and 200 ms in the ISI histograms, respectively. The total numbers of intervals were obtained from the ISI histograms with a binsize of 15 ms. **B:** ISI density for intervals of 100 ms and 200 ms length, taken from ISI histograms with a temporal resolution of 5 ms. The high variance of the deduced data prevented appropriate fits (see Section 2, Methods). However, a linear regression revealed an slight increase in the corresponding coherence measures in all cases. **C:** The SNR* measure as a function of the background amplitude. The number of evoked spikes in a time interval of length 10 ms after each stimulus was cumulated to yield SNR*.

the properties of the dendritic AMPA synapses. This way the balance between inhibitory and excitatory influences on the system's dynamics was directly affected.

The firing frequency was changed in the range $0.5\ \mathrm{Hz} \leq \nu_{\mathrm{exc}} \leq 2.0\ \mathrm{Hz}$ with a stepsize of $\Delta\nu_{\mathrm{exc}} = 0.1\ \mathrm{Hz}$, whereas ν_{inh} was kept fixed at 5.5 Hz. As in the conductance study, we investigated the impact

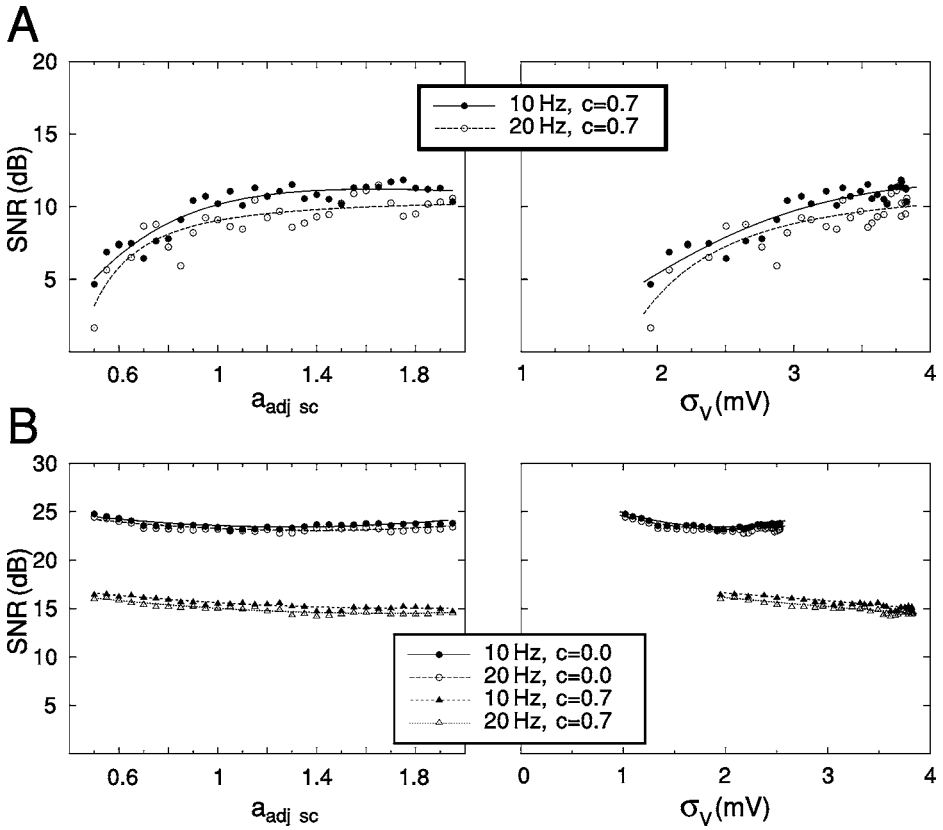

Figure 4. SNR obtained from the PSDs by varying quantal conductances. Model corresponding to medium excitability. **A:** SNR following from the PSDs at 10 Hz and 20 Hz in the spike train power spectra for $c = 0.7$. **B:** SNR following from the power spectra analysis of the voltage records. The SNR deduced from the peaks at 10 Hz and 20 Hz for $c = 0.0$ and $c = 0.7$ stays constant over the whole simulated background parameter range, indicating that the background does not affect the response of the cell with respect to V_m changes caused by the periodic stimulation.

of the background correlation by performing simulations with $c = 0.0$ and $c = 0.7$. All simulations were done using channel densities corresponding to medium excitability.

The observed effects of a change in ν_{exc} on V_m were qualitatively similar to that obtained in the conductance study. First, increasing ν_{exc} led to a continuously increasing depolarization slightly larger than that observed in the conductance study (between -70 mV and -58 mV for $c = 0.0$, between -70 mV and -60 mV for $c = 0.7$). The average V_m showed also a saturation behavior by converging toward a constant value for high ν_{exc}. Second, the amplitude of V_m fluctuations increased for stronger backgrounds (1 mV $\leq \sigma_V \leq$ 3 mV for $c = 0.0$, 2 mV $\leq \sigma_V \leq$ 3.5 mV for $c = 0.7$, see Fig. 5A). Higher correlation led to higher σ_V but, in contrast to the conductance study, also affected the range of voltage fluctuations. For both cases, σ_V reached the same amplitude for high ν_{exc}. Third, although additional stimulation led to an increase of the V_m fluctuations that was slightly higher than in the conductance study, the differences between σ_V obtained from noise-only and noise-plus-stimulus simulations vanished for higher background strength. Last but not least, the average V_m after stimulus (see Fig. 5B) as well as the PSTHs show behaviors similar to what we found in the conductance study.

The number of spikes evoked at the soma was much higher than in the conductance study. Although for $c = 0.0$ up to $\nu_{\text{exc}} \sim 0.9$ Hz the system remained subthreshold, after that the spike rate increased constantly to about 35 Hz in the noise-only as well as noise-plus-stimulus simulations. For $c = 0.7$ it was slightly higher (about 45 Hz in both cases for $\nu_{\text{exc}} =$ 2.0 Hz), and spikes were evoked also for lower ν_{exc}.

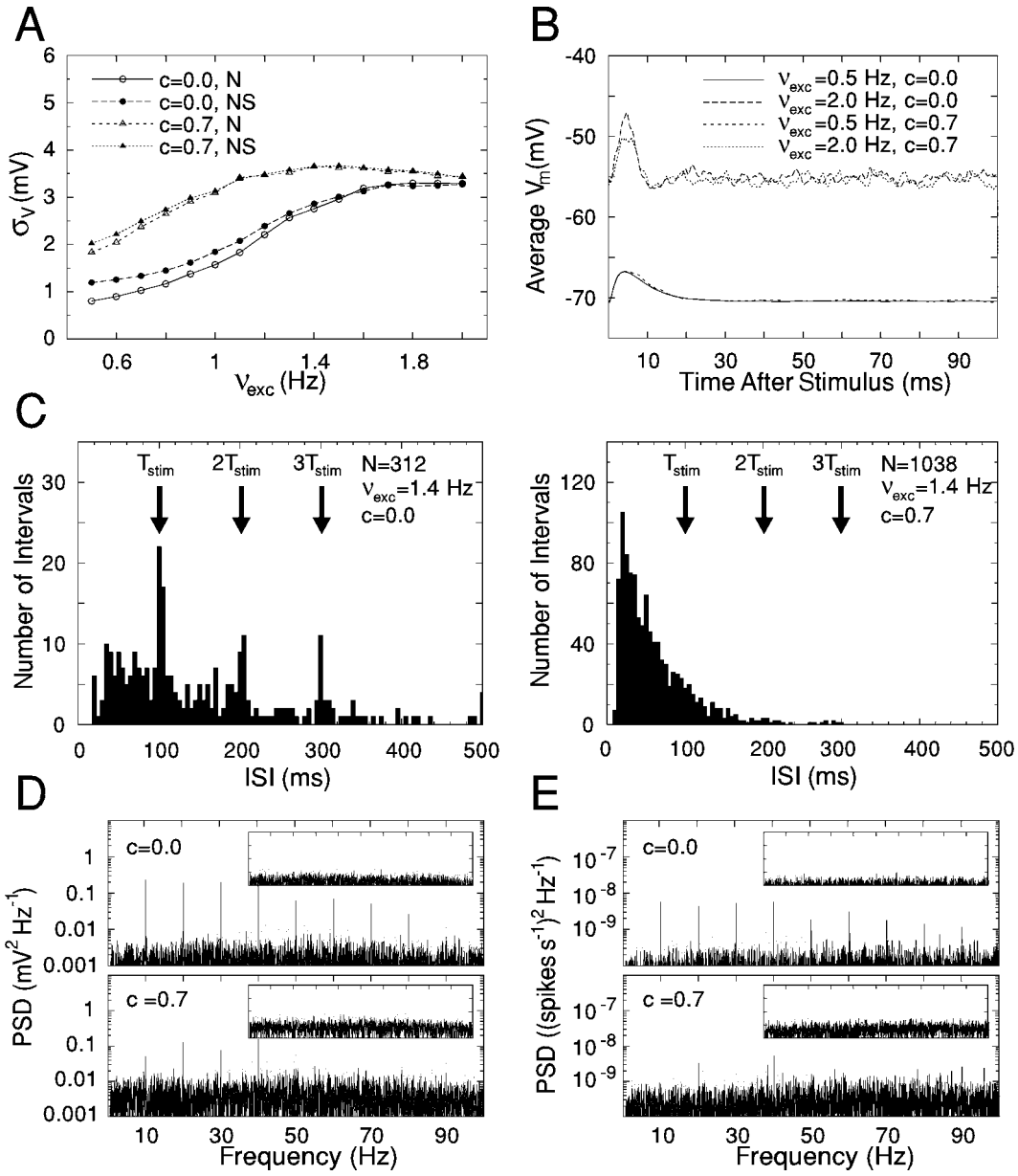

Figure 5. Behavior of the model for variations in the release frequency of excitatory synapses. **A:** Impact of the excitatory background firing rate on V_m fluctuations. The plot shows the behavior of σ_V as a function of ν_{exc} for simulations with background noise-only (N) as well as noise-plus-stimulus (NS) for $c = 0.0$ and $c = 0.7$. **B:** Average V_m after stimulation for the two limiting frequency settings for both correlation values. **C:** Representative ISI histograms obtained from noise-plus-stimulus simulations with $\nu_{\text{exc}} = 1.4$ Hz for $c = 0.0$ (left plot) and $c = 0.7$. The distribution in the zero correlation case shows clear peaks at multiples of the stimulation period of 100 ms, whereas the corresponding distribution for higher correlations matches that for a Poisson-like processes. **D** and **E:** Representative PSDs of voltage records (D) and spike trains (E) for $\nu_{\text{exc}} = 1.4$ Hz obtained from noise-plus-stimulus simulations for both cases. The inlets show the corresponding PSDs calculated from the noise-only simulations. Channel densities corresponding to medium excitability were used in all cases.

Moreover, in this case the ISI histograms for $c = 0.0$ show clear peaks at multiples of the stimulation period (Fig. 5C, left plot) in the middle ν_{exc} range before for higher frequencies the background, expected from Poisson-spike trains with refractory period, blot out that peaks. For $c = 0.7$ this background in the ISI histograms was much stronger (Fig. 5C, right plot).

For both correlation values, the PSDs of spike trains and voltage records (Fig. 5D and E) show a behavior similar to what we found in the conductance study. The spectral noise increases with higher ν_{exc} and, for fixed ν_{exc}, is higher for $c = 0.7$. Whereas the height of the peaks at multiples of the signal frequency continuously increases in the case of the voltage PSDs, the height of the peaks in the spike train PSDs goes through a maximum for increasing ν_{exc}.

To quantify this rather qualitative picture of a SR-like behavior, we applied again all introduced measures of response coherence (Figs. 6 and 7). Both COS and ISID show clear resonance peaks for intermediate background strength. As expected, the strongest peaks

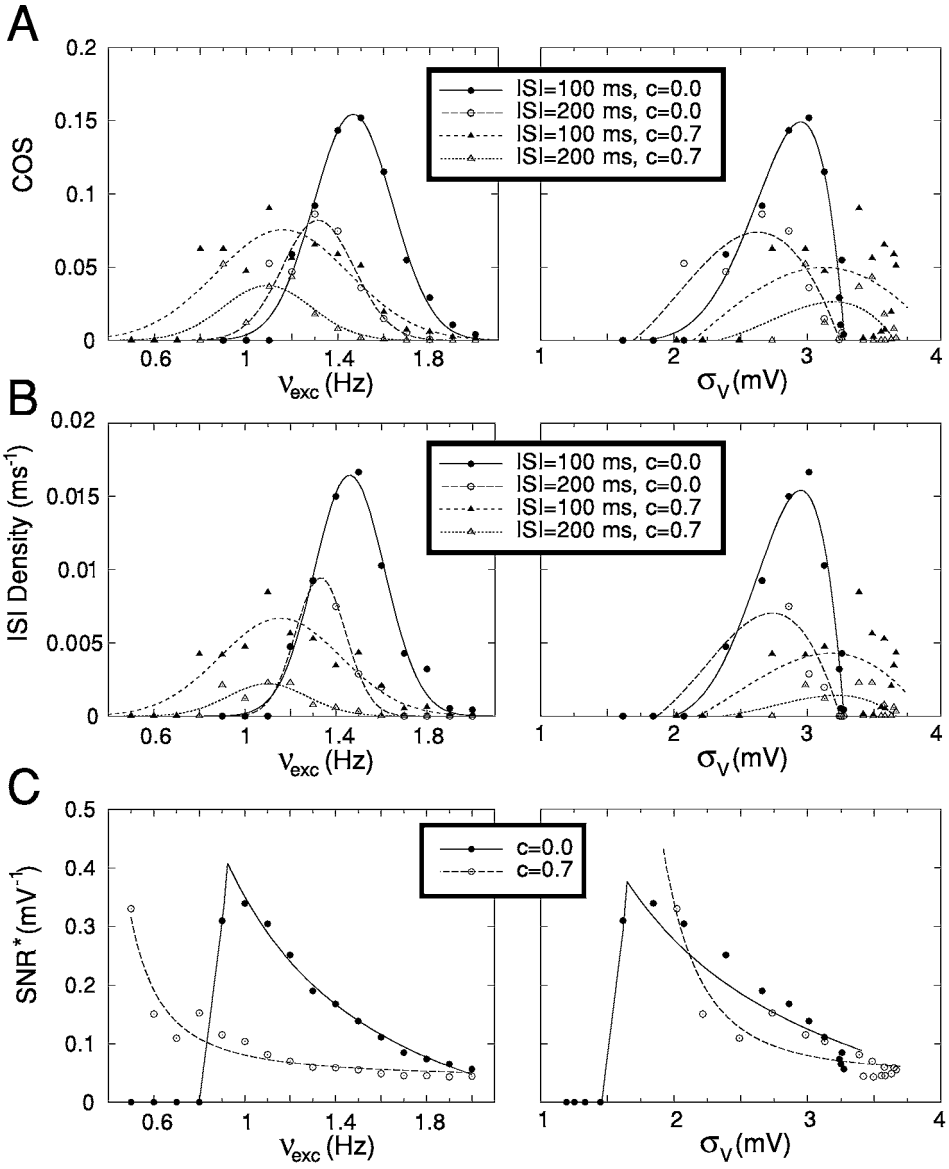

Figure 6. Classical stochastic resonance obtained by varying the release frequency of excitatory synapses. The left plots show the coherence measures as a function of the background amplitude labeled ν_{exc}. The right plots depict the corresponding measures as a function of the amplitude of V_m fluctuations. **A:** COS obtained from the first- and second-order peaks at 100 ms and 200 ms in the ISI histograms, respectively. The total number of intervals were obtained from the ISI histograms with a binsize of 15 ms. **B:** ISID for intervals of 100 ms and 200 ms length, taken from ISI histograms with a temporal resolution of 5 ms. **C:** SNR* as a function of the background amplitude. Medium excitability in all cases.

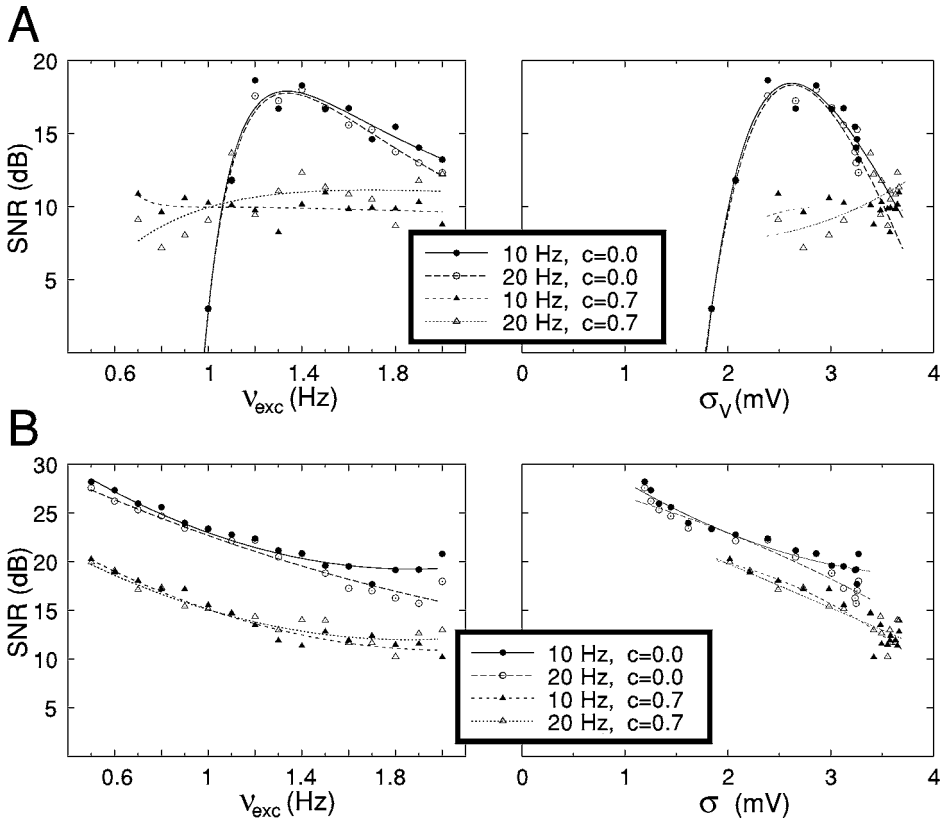

Figure 7. Different measures of signal-to-noise ratio when varying the release frequency of excitatory synapses. The SNR is shown for the PSDs of the first and second peaks at 10 Hz and 20 Hz, respectively, in the appropriate power spectra for the model with medium excitability, and with $c = 0.0$ and $c = 0.7$. **A:** SNR following from spike train power spectra. In the zero correlation case, there is a clear increase and decrease in the SNR, indicating a SR-like behavior in the system's coherent response. In contrast, for $c = 0.7$ the SNR stays constant over the simulated range of background strength. **B:** SNR following from the power spectrum analysis of the voltage records. The ratios decrease for increasing background strength due to the higher V_m fluctuations and, thus, internal noise in the system that blot out the effects of the periodic stimulus.

come from the ISIs of length equal to T_{stim}. ISIs of higher order lead to smaller peaks but also show a clear SR-like behavior. For $c = 0.7$ the height of the peaks is much smaller. This can be understood by noting that here the coherence between periodic stimulus and response is disturbed by the spontaneous evoking of spikes due to the background, which is much stronger when correlation is present.

Another remarkable result is that the maxima of the resonance peaks in the various cases do not match. We observed that maximal coherence is reached at lower ν_{exc} values for higher-order peaks. Moreover, higher correlation shifted the resonance peaks toward lower frequencies. In contrast, due to the nonlinear relationship between σ_V and ν_{exc} (Fig. 5A), the maxima were taken for higher values of σ_V when correlation was present. Focusing on the strongest peak, COS as well as ISID take their maxima at comparable values—namely, $\nu_{\text{exc}} \sim 1.5$ Hz and $\sigma_V \sim 3.0$ mV for $c = 0.0$, $\nu_{\text{exc}} \sim 1.2$ Hz and $\sigma_V \sim 3.5$ mV for $c = 0.7$. The latter is equal to the σ_V for maximal coherence we found in the conductance study.

For the probability measure (Fig. 6C), the same argumentation applies as in the case of the conductance study. The steplike structure is clearly visible for $c = 0.0$, where for low background noise amplitudes the system stayed subthreshold and spontaneous firing started when the background amplitude ($\nu_{\text{exc}} \sim 0.8$ Hz) or the resulting V_m fluctuations ($\sigma_V \sim 1.5$ mV) were strong enough to cross in conjunction with the additional stimulus this threshold. For higher correlations, even low ν_{exc} together with the periodic stimulation forced the cell to fire. Therefore, in the simulated parameter range only a decrease of SNR* was obtained.

Comparing this finding with the corresponding result in the conductance study ($\sigma_V \sim 1.7$ mV) supports the idea that the probability measure quantifies the onset of a coherent response of the system, which must not occur at the same fluctuation level for different model parameter settings, in contract to its SR-like behavior.

The PSDs of the spike trains indicated a SR-like behavior only for $c = 0.0$ (Fig. 7A). Here, a sharp increase of the SNR is followed by a rather slow decrease. Remarkably, the behaviors deduced from the second- and higher-order peaks (data not shown) in the power spectra follow quantitatively and qualitatively that obtained from the peak at the signal frequency of 10 Hz. In contrast, the SNRs for higher correlations remain nearly constant over the simulated parameter range.

Finally, we investigated the SNR following from the voltage PSDs. In contrast to the conductance study, the calculated SNR continuously decreases for higher noise amplitudes, which, however, is the expected behavior. Due to the disturbance of the balance between inhibition and excitation, there was no compensating increase of inhibitory influences that could reduce the effects of noise coming from the excitatory inputs. This way, the internal noise was determined mainly by the excitatory background and blotted out the effects on V_m due to additional stimulation.

3.3. *Correlation Study: The Impact of the Background Statistics*

The results presented above, in conjunction with recent modeling investigations (e.g., Destexhe and Paré, 1999), revealed that the correlation in the background significantly impacts the amplitude of the V_m fluctuations. Therefore, it is natural to ask if a change of this correlation leads to a similar SR-like behavior in the coherence of the cell's response.

To investigate the effects of the correlation, the parameter c was changed in the interval $0.0 \leq c \leq 0.99$ with a stepsize of $\Delta c = 0.05$ for $c \leq 0.90$ and $\Delta c = 0.01$ for $c > 0.90$. Three models with parameter settings leading to a different membrane excitability were investigated—namely, low ($a_{\text{ic}} = 0.4$), mid ($a_{\text{ic}} = 0.7$) and high ($a_{\text{ic}} = 1.0$).

For all three models, the V_m showed a similar behavior as a function of c. Up to $c \sim 0.9$, V_m took values around -65 mV and only slightly depolarized with increasing c. For the highest values of the correlation, the V_m dropped rapidly due to the increasing influence of fluctuations (Fig. 8A). Fig. 8B shows the average V_m after stimulus for various settings. The influence of the membrane excitability on the average V_m was found to be minimal. In contrast to the conductance study and the frequency study, the voltage fluctuations increased continuously with increasing background amplitude. More interesting, however, is the fact that the observed range of V_m fluctuations was much larger but decreased for higher excitability (1 mV $\leq \sigma_V \leq$ 7.5 mV for low excitability, 1.5 mV $\leq \sigma_V \leq$ 6.5 mV for medium excitability, 2 mV $\leq \sigma_V \leq$ 5.5 mV for high excitability). This finding is quite remarkable because one would expect that a higher excitability leads to higher fluctuations for fixed input amplitudes. Last but not least, as in the case of the frequency study, the additional subthreshold stimulations only minimally affected σ_V. Whereas with stimulation σ_V increased about 0.5 mV for low correlation settings, the effects due to stimulation vanished for higher c.

Because of the much higher σ_V, the number of spontaneously elicited spikes, and, thus, the total number of spikes was (on average) higher than in the preceding studies. Whereas in the low-excitable model we recorded no spikes in the simulated time interval up to $c \sim 0.65$, afterwards it increased constantly to finally yield a firing rate of about 25 Hz for both noise-only and noise-plus-stimulus simulations. For medium and high excitability, however, spontaneously generated spikes appeared even for zero correlation. In this case, we observed values between 0.1 Hz and 45 Hz (medium excitability) as well as 4 Hz and 50 Hz (high excitability).

Despite this high number of spike events for medium and high excitability, indications for peaks at multiples of the signal period in the corresponding ISI histograms were only rare. Two representative examples are shown in Fig. 8C. With low excitability, the calculation of statistically reliable ISI histograms was possible only for higher c. These, however, took the shape expected for ideal Poisson-like spike trains, and no clear indication for peaks was found.

The PSDs (Fig. 8D and E) show the expected behavior. First, for all three models the periodic depolarization of the membrane led to clear peaks in the voltage power spectra with decreasing height and increasing spectral noise for higher c. Second, the spike train PSDs also show peaks at signal frequency and multiples of it. However, whereas at medium excitability the height of the peaks runs through a maximum, it decreases only for low and high excitability for

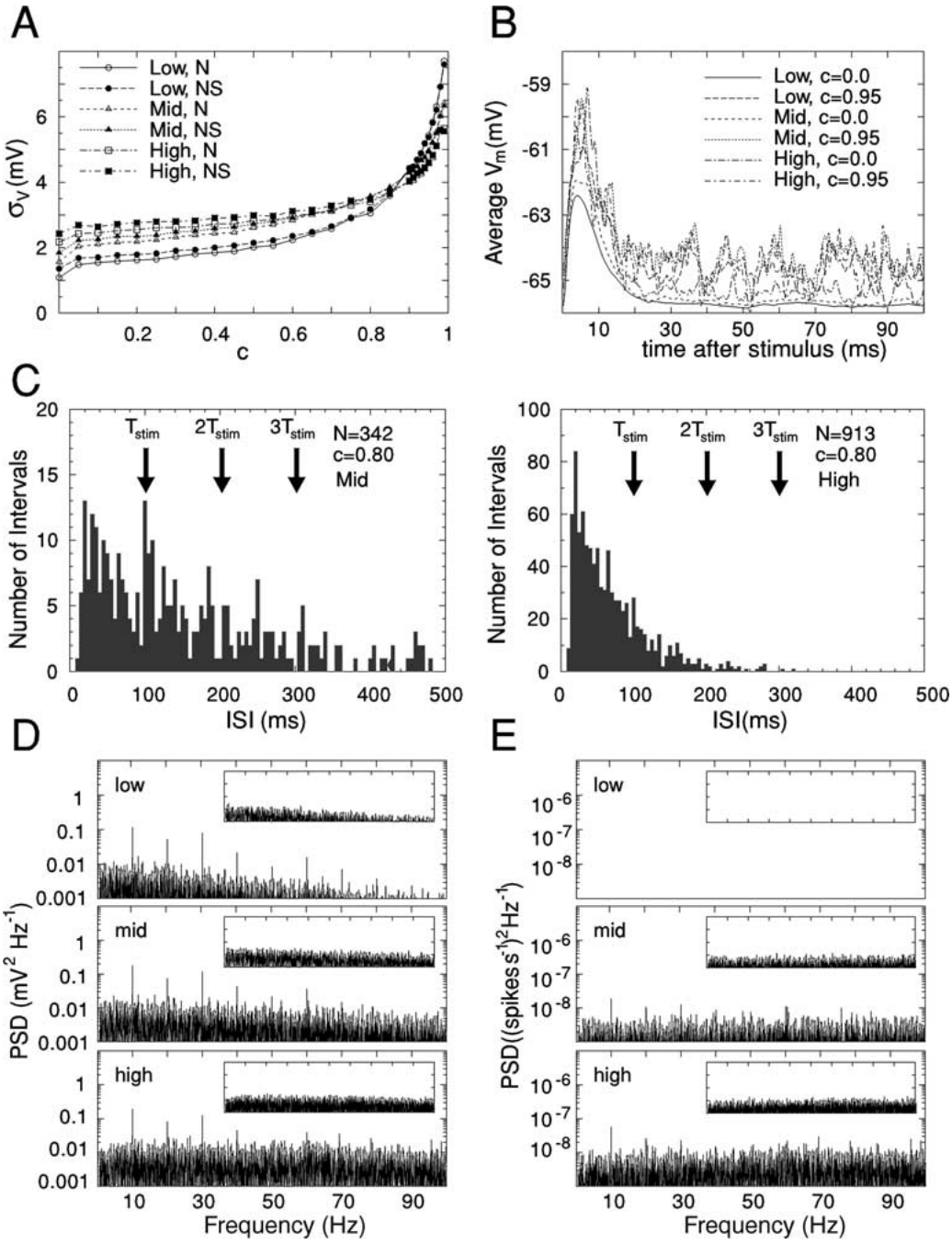

Figure 8. Behavior of the model for variations in the correlation of excitatory and inhibitory synapses. **A:** Impact of the background correlation on V_m fluctuations quantified by σ_V. The plot shows the behavior of σ_V as a function of c for simulations with noise-only (N) as well as with noise-plus-stimulus (NS) for three levels of excitability: low, medium (mid), and high. In contrast to the conductance study and frequency study, the fluctuations increase rapidly for higher correlation settings and do not saturate. **B:** Average V_m after stimulation for both correlation settings in the three models. **C:** Representative ISI histograms obtained from noise-plus-stimulus simulations with $c = 0.8$ for the medium and high excitability. The distribution obtained for medium excitability shows indications for peaks at multiples of the stimulation period, whereas the corresponding distribution for high excitability matches that of a Poisson-like processes with refractory period. **D** and **E:** Representative PSDs of voltage records (D) and spike trains (E) obtained from noise-plus-stimulus simulations for the three models ($c = 0.8$ for each case). The inlets show the corresponding PSDs calculated from the noise-only simulations.

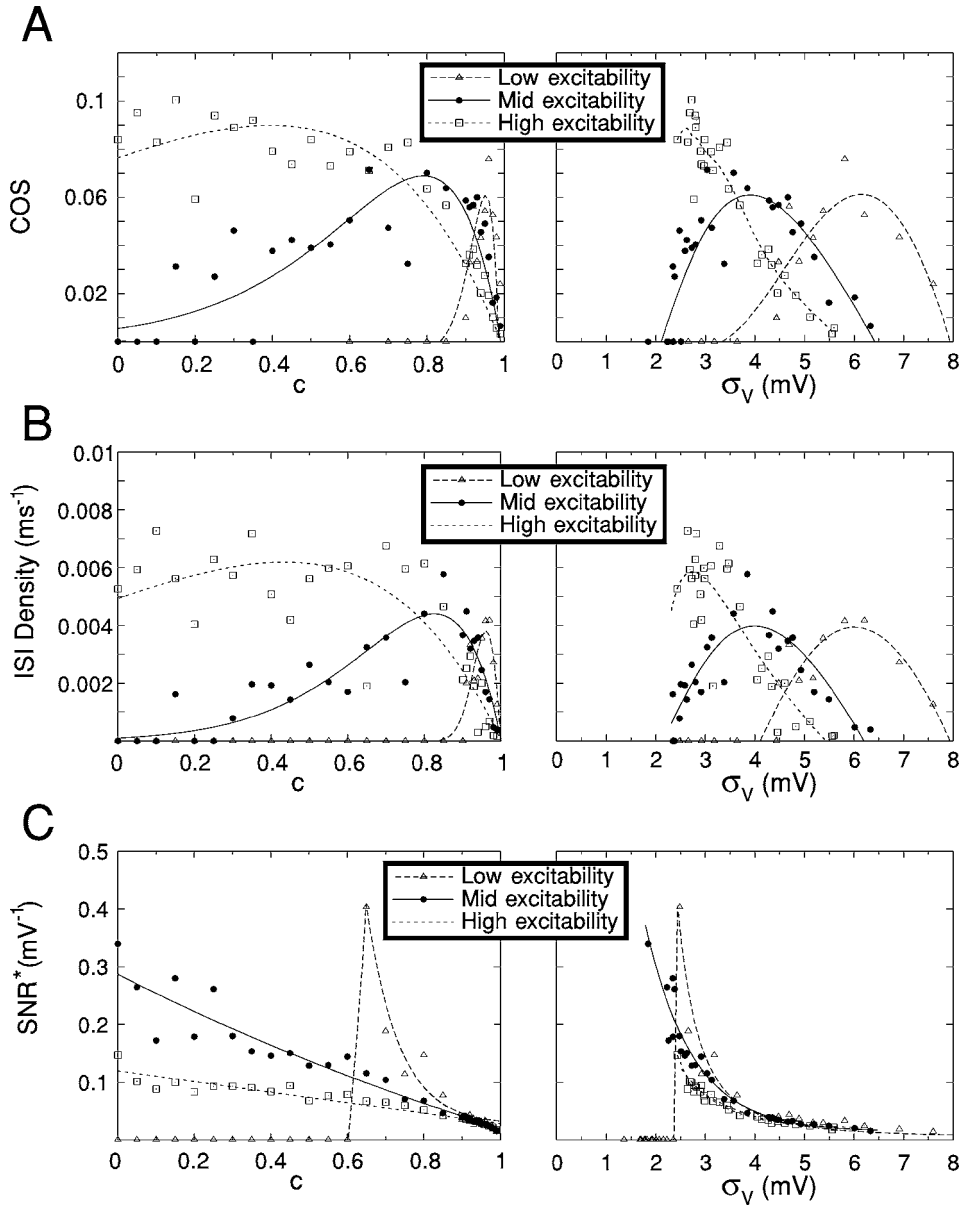

Figure 9. Resonance in the coherent response as a function of correlation for different levels of membrane excitability. The left plots show the coherence measures as a function of c. The right plot depicts the corresponding measures as a function of σ_V resulting from background and stimulus inputs. **A:** Coherence between output and stimulus corresponding to the first peak at 100 m in the ISI histograms. The total numbers of intervals were obtained from the ISI histograms with a binsize of 15 ms. **B:** ISI density for interval of 100 ms length. The ISI densities were taken from the histograms with a temporal resolution of 5 ms. **C:** SNR* as a function of the background amplitude. The number of evoked spikes in a time interval of length 10 ms after each stimulus was cumulated to yield SNR*.

increasing background amplitude. With low excitability, PSDs could be obtained only for higher c.

Figures 9 and 10 depict the results of the applied measures of coherence. COS as well as ISID show peaks that become most clear when the corresponding measures are plotted as functions of σ_V. Whereas with high excitability we observed only the decreasing branch of the coherence curve, with medium and low excitability these quantities took their maxima at some intermediate values—namely, $c \sim 0.95$ and $\sigma_V \sim 6$ mV at low excitability, and $c \sim 0.75$ and $\sigma_V \sim 4$ mV at medium excitability. The latter value is

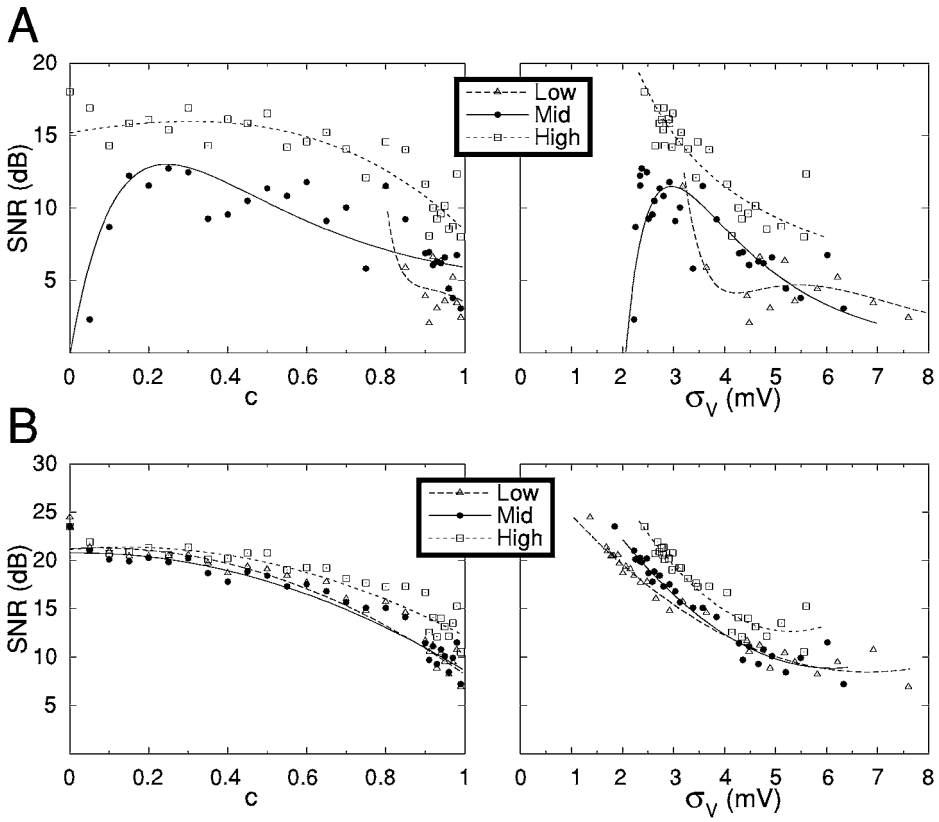

Figure 10. SNR obtained from the PSDs in the correlation study. The left plots show the measures as a function of the background amplitude labeled by c, whereas the right plots depict the corresponding measures as a function of σ_V. **A:** SNR following from spike-train power spectra. A SR-like behavior is visible only for medium excitability, whereas with low and high excitability, the corresponding SNRs decrease only with increasing background strength. **B:** SNR following from the power spectrum analysis of the voltage records. As for the frequency study, the corresponding SNRs decrease for all models due to the higher V_m fluctuations caused by the background, which interfere with the periodic depolarization caused by the stimulation.

quite remarkable because it comes close to the amplitude of V_m fluctuations for which we observed maxima in the conductance and frequency studies. Lowering the excitability shifted the peak toward higher background amplitudes due to the fact that higher fluctuations are needed to cross the threshold for generating spikes. A second observation concerns the height of the peaks, which decreases for decreasing excitability. Because the strength of the weak periodic input was kept constant during the simulations, their impact on the cell is lower for low excitability. However, an expected impact of the excitability on the width of the resonance peaks due to the decreasing of the covered σ_V range with increasing excitability (see above) could not be deduced from the data.

Only with low excitability the model yielded a probability measure that shows a sharp step at some value of the background amplitude ($c \sim 0.6$, $\sigma_V \sim 2.5$ mV, Fig. 10C). In contrast, for medium and high excitability, spikes in coherence with the additional stimulus were elicited even for zero correlation, leading only to a decrease of the SNR*. As expected, the probability and the related SNR* were higher for medium excitability due to the weaker influence of the background.

Only for medium excitability the SNR obtained from spike train PSDs displays a SR-like behavior (Fig. 10A). For low excitability, the statistics prevents an equivalent conclusion. In the highly excitable model, we observed a continuous decrease of the SNR following the same reasoning as given above for the probability measure. The analysis of the PSDs of the voltage records (Fig. 10B) shows that, in all three models the SNR decreases for increasing background amplitudes.

3.4. *Robustness of Stochastic Resonance-Like Behavior*

We verified the robustness of our observations by varying a number of parameters in the model. In addition to testing different levels of dendritic excitability and different parameters for the background activity (see above), we tested whether the presence of SR was dependent on the particular set of voltage-dependent conductances present. In addition to I_{Na}, $I_{\mathrm{K\,d}}$, and I_{M} voltage-dependent currents, a Ca^{2+}-dependent potassium current (C-current) $I_{\mathrm{K\,Ca}}$ (Yamada et al., 1989) and a high-threshold Ca^{2+}-current (L-current; McCormick and Huguenard, 1992) $I_{\mathrm{Ca\,L}}$ with conductance densities corresponding to low excitability were used. Although the overall range of V_m fluctuations was increased ($2\ \mathrm{mV} \leq \sigma_V \leq 11\ \mathrm{mV}$), the COS measure shows a clear increase and decrease in the response coherence (Fig. 11A), indicating that the SR-like effect is only minimally affected by additional Ca^{2+}-dependent conductances. The optimal coherence was reached for $\sigma_V \sim 6$ mV, in accordance with the findings in the correlation study.

Another set of voltage-dependent conductances with different kinetics (Migliore et al., 1999) was also tested, including sodium and delayed-rectifier

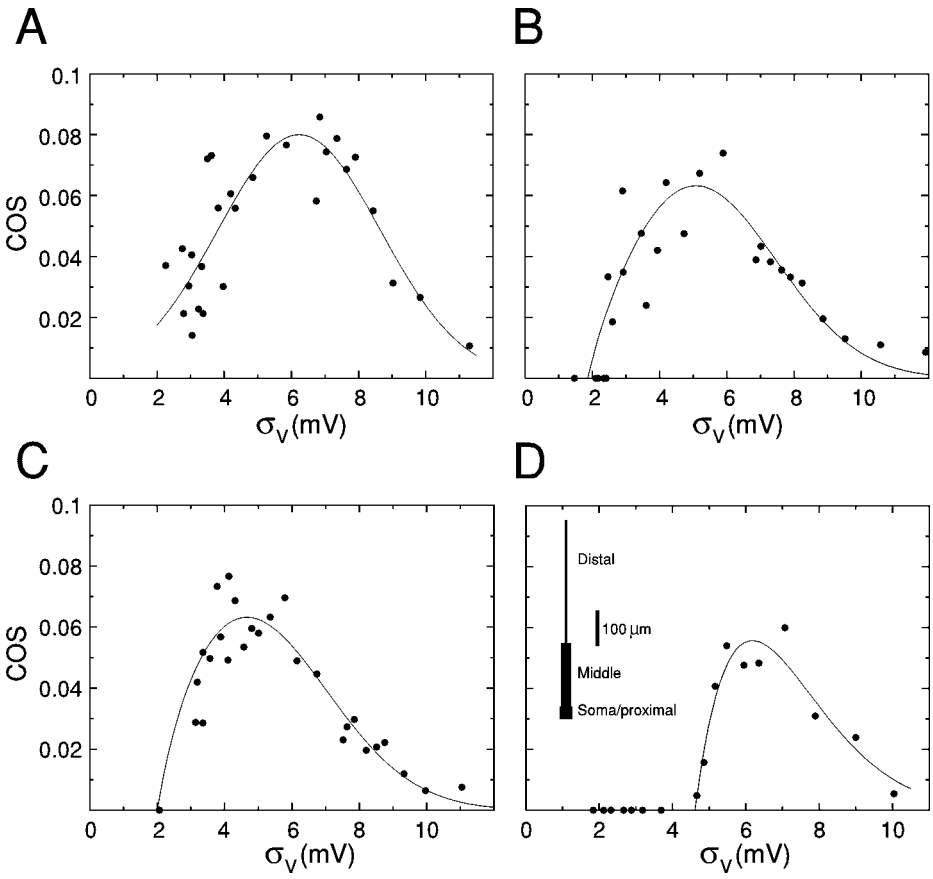

Figure 11. Physiological robustness of the resonance in the response coherence to an additional applied subthreshold periodic stimulus. **A:** Additional Ca^{2+}-dependent potassium current and a high-threshold Ca^{2+}-current in conjunction with I_{Na}, $I_{\mathrm{K\,d}}$, and I_{M} voltage-dependent currents lead to a resonance in the response coherence (quantified by the COS measure), with optimal coherence is reached for $\sigma_V \sim 6$ mV, in accordance with the findings in the correlation study. **B:** Resonance behavior for a model with voltage-dependent conductances including sodium and delayed-rectifier potassium channels, as well as A-type potassium channels $I_{\mathrm{K\,A}}$ with conductance densities corresponding to medium excitability (see Section 2, Methods). **C:** The COS measure as a function of internal V_m fluctuations for a model with active conductance settings according to B and additional persistent sodium channels. **D:** A three-compartment model (left panel) with membrane area and conductance settings corresponding to the detailed model leads to a clear resonance behavior of the COS measure as a function of the internal noise quantified by σ_V.

potassium channels, as well as an A-type potassium current $I_{\mathrm{K\,A}}$ with conductance densities adjusted to match the general behavior of the medium excitable model described above. Also here the range of V_m fluctuations was increased (1.5 mV $\leq \sigma_V \leq$ 12 mV), but the COS measure shows a clear resonance peak (Fig. 11B). The optimal coherence was reached for $\sigma_V \sim 5$ mV, which is slightly higher than that found in the correlation study. These findings remained nearly unaffected when an additional persistent sodium current (French et al., 1990; Huguenard and McCormick, 1992) was incorporated into the model (Fig. 11C).

The impact of the morphology of the cell on the SR effect was also addressed. To this end, we used a simplified three-compartment model with membrane area corresponding to the total membrane area of the detailed pyramidal cell (Destexhe, 2001). The voltage-dependent current I_{Na}, $I_{\mathrm{K\,d}}$, and I_{M} used for the model had densities leading to an average V_m as well as V_m fluctuations corresponding to the low excitable model. Also here the COS measure follows a resonance-like behavior as a function of the internal noise, with an optimal coherence at $\sigma_V \sim 6$ mV, which matches that found in the correlation study.

4. Discussion

In this article we have investigated the presence of stochastic resonance in detailed biophysical models of a morphologically reconstructed neocortical pyramidal neuron in the presence of excitatory and inhibitory synaptic background activity. The chosen (correlated) Poisson-like distributed background activity was adjusted to match the results found in recent measurements in cat parietal cortex in vivo (Destexhe and Paré, 1999; Paré et al., 1998). The impacts of various background properties (quantal synaptic conductances, firing rate and correlation) and physiological settings (active conductances, morphology) on the responsiveness were studied. In all three cases we observed clear indications for a behavior consistent with the SR phenomenon, depending on the measure used to quantify the response coherence of the model, as well as how the "noise" is affected.

4.1. Measures of Response Coherence and Their Applicability

Not all measures of response coherence used here (see Section 2, Methods) show a resonance-like behavior. The measures deduced directly from the spike trains via the corresponding ISI histograms—namely, ISID (Eq. (2)) (see Douglas et al., 1993; Ivey et al., 1998; Longtin, 1993; Wiesenfeld and Moss, 1995) and COS (Eq. (3)) (see Chialvo and Apkarian, 1993) show the most clear indications for resonance peaks, whereas the SNR calculated from the spike train PSDs (Eq. (1)) (e.g., Fauve and Heslot, 1993; Lee and Kim, 1999; Wiesenfeld and Moss, 1995; Zhou and Moss, 1990) only partly allowed such an interpretation. Even modifications of the mathematical definition of the SNR lead to not enhancement of this result. This is easy to understand because spikes represent a low statistics compared to the subthreshold voltage fluctuations (only ∼2% of the time is spent producing spikes for a cell firing at 10 Hz, and only few of these spikes are related to the stimulus). In addition, PSD analysis via the fast Fourier transform was accompanied by a large procedure-dependent error. This could be minimized by using more complex analysis methods—e.g., fast Fourier transforms with overlapping data segments and windowing (Press et al., 1993). However, the necessary computational expenditure can be circumvented by using quantities that deal in a direct way with the spike times, such as COS or ISID.

On the other hand, the probability measure P_{spikes} (Eq. (4)), derived from the PSTH, and its corresponding SNR^* (Eq. (5)), are less suitable to show SR-like behavior in the response coherence. Following the reasoning outlined above, due to a sharp step followed by an exponential decrease, they are rather quantifying the background amplitude at which a coherent response of the system starts. As our simulations have shown, this onset must not occur at the same amplitude of V_m fluctuations for models with different parameter settings. Moreover, we found that the functional behavior of the probability measure is much more sensitive on the model parameters. Only in a few number of cases we obtained a step within the range of the simulated background amplitudes.

4.2. "Classical" Stochastic Resonance in Pyramidal Neurons

If one associates background activity with "noise," and if the amplitude and strength of this noise are varied by conventional ways (frequency of release events, quantal conductances), then the present results provide evidence for phenomena that can be associated with SR in its classical sense—namely, an enhancement of the

response in coherence with additionally applied weak stimulation for a particular range of noise strength (Benzi et al., 1981; Fauve and Heslot, 1993; Longtin et al., 1991).

In the conductance study, the coherence in the response increased for higher quantal conductances, and reached a maximum for a certain amplitude of the background (Fig. 3A and B). However, even for very high conductances there was no clear decrease of the response coherence. We suggest that the reason for this can be found in the observed saturation property of σ_V because of which the V_m fluctuations converged toward a fixed value (Fig. 2B). For zero correlation the very low number of elicited spikes prevented a statistical analysis. However, we found the remarkable property of a nearly constant SNR deduced from voltage PSDs over a broad range of background amplitudes (Fig. 4B). It seems that an increase in the background activity has had no effect on the response of the cell with respect to V_m changes caused by the additional input. This can be traced back to the fact that the balance between inhibitory and excitatory influences was not affected by the present parameter settings.

In the frequency study, although the V_m fluctuations showed a saturation behavior that was qualitatively and quantitatively comparable to what we observed in the conductance study (Fig. 5A), a change in ν_{exc} led to full resonance peaks (Fig. 6A and B). Moreover, here a direct comparison between the two correlation settings was possible. First, for $c = 0.0$ the peaks in the COS and ISID plots were higher than for $c = 0.7$. This can be explained by the fact that higher correlations caused a higher number of spontaneously evoked spikes, which interfered with the spikes elicited in synchrony with the stimulus. Second, when depicted as functions of the σ_V, for $c = 0.0$ the resonance peak was shifted toward lower values, whereas for $c = 0.7$ the maxima of the COS and ISI density measures were taken for a σ_V, which compares to that found in the conductance study. It is remarkable that the resonance behavior showed up in the SNR deduced from the spike-train power spectra only for low correlations (Fig. 7A). For $c = 0.7$ the SNR stayed nearly constant over the simulated ν_{exc} range. The SNR calculated from the voltage PSDs (Fig. 7B) shows, in contrast to the conductance study, the expected decrease for increasing noise amplitudes.

These results underline the findings of a recent investigation of rat hippocampal CA1 neurons (Stacey and Durand, 2000), which point out the impact and role of noise in central neurons in the framework of the SR phenomenon.

4.3. *"Nonclassical" Stochastic Resonance*

A clear resonance in the coherence of the cell's response was also found when the correlation and thus the statistics of the synaptic background were changed. Although the influence of correlation in the noise on the behavior of simple neuron models was discussed previously (e.g., Capurro et al., 1998; Gerstein et al., 1989; Mar et al., 1999; Mato, 1998), our study goes further by showing that a change in the correlation itself gives rise to a SR-like behavior. This novel form of SR departs from the classical notion of stochastic resonance because here the response of the system is enhanced not by an optimal noise strength but instead by optimal statistical properties of the synaptic background noise.

Three cases with different levels of membrane excitability were investigated. Whereas in the high excitable model the huge number of spontaneously evoked spikes even for lowest correlations led only to a decrease in the coherence measures, full resonance peaks could be deduced from medium and low excitability (see Fig. 8A and B). Here, lower excitability shifted the curves toward higher c because higher fluctuations were needed to cross the threshold for spike generation. For higher excitability we observed an increase in the height of the resonance peaks, which can be explained on the same basis. Remarkably, the maximum for the medium excitability was taken for values of σ_V that match that found in the frequency and conductance studies. A resonance behavior only marginally appeared in the SNR obtained from the spike train PSDs (Fig. 10A). The SNR obtained from the voltage record (Fig. 10B) matches the behavior found in the frequency study.

4.4. *Possible Functional Consequences*

In all cases corresponding to the medium excitability investigated here, the maximal coherence was reached for comparable amplitudes of V_m fluctuations—namely, $3.5\ \text{mV} \leq \sigma_V \leq 4\ \text{mV}$. It is interesting to note that these values are covered by the range of fluctuations found in measurements in vivo—namely, $\sigma_V = 4.0 \pm 2.0\ \text{mV}$ (Destexhe and Paré, 1999). Moreover, the resonance-like behavior was only minimally affected

by various physiological settings, including active conductances and morphology. These findings underlines what we have proposed earlier (Hô and Destexhe, 2000): the V_m fluctuations that, at first glance, can be viewed as noise inherit to the system influence in a direct way the responsiveness of the cell by interfering with the effects caused by additional stimuli, independent of the nature of their driving forces.

However, the above-stated interpretation of our findings in the framework of classical SR has to be done with greatest care. In central neuronal systems, the question about how noise impacts the response of neuron rather has to be replaced by a more ambitious one: How does the overall synaptic input information provided to a neuron affects the response behavior of that neuron with respect to special aspects in this input information? In other words, if one assumes that background activity is made of the superposition of many independent—or weakly correlated signals, then the properties shown here imply that the responsiveness to anyone of these signals is enhanced by the presence of the other signals, which in our case play the role of "noise." This implies that the neuron could in principle process and transmit many independent signals in parallel, much more efficiently than transmitting them individually. How this property is implemented at the level of populations of interconnected neurons is an open question that should be addressed in future models.

This picture goes beyond what can be achieved from an interpretation based on the classical SR picture. First, there is no longer a distinction between noise and signal. Here we rather distinguish between various properties and, thus, the contents of the overall information provided as input. The behavior and the response of the system are determined by special aspects in that input information and can be focused on some particular aspects of it. Second, a single neuron can no longer be treated as an independent entity. It is merely a part of a large network whose dynamics impacts the local dynamics of the neuron. In turn, the single neuron's dynamics may impact the network level. Thus this dynamic feedback loop between "signal" and "noise" can be viewed as a new kind of resonance, caused and determined by the local and global dynamics of the system in question, justifying the term *dynamical resonance*.

In the framework of this model, a lot of questions must be left unanswered. To mention only a few: Where does the correlation comes from? How do particular aspects and properties of the dynamics of the system manifest in spike trains? Besides the correlation, do there exist other aspects of the information provided that can affect the behavior of single neurons? If so, how? Can a dynamical mechanism described above lead to a stable system? These problems cannot be solved on the single-cell level but only in the framework of networks with more realistic behaving constituents. Also the question about the impact of the signal properties and the range of physiological and morphological parameters that give rise to the described resonance phenomena need a much more detailed investigation.

In conclusion, the present computational investigation allows us to give an answer to the question in the main title: Yes, under a certain restrictive point of view, cortical pyramidal neurons are subject to phenomena that fit into the framework of SR. However, put into a slightly more general context, the results obtained so far also reveal a way that goes beyond this interpretation and can be viewed as a small step toward a deeper understanding of the stochastic aspects of neuronal dynamics and information processing in the cerebral cortex.

Acknowledgments

Research supported by the CNRS, the Medical Research Council of Canada (MT-13724) and the National Institutes of Health (R01-NS37711). We thank Nicolas Hô for stimulating discussions.

References

Azouz R, Gray C (1999) Cellular mechanisms contributing to response variability of cortical neurons in vivo. J. Neurosci. 19:2209–2223.

Benzi R, Suter A, Vulpiani A (1981) The mechanism of stochastic resonance. *J. Phys.* A14:L453–L457.

Bezrukov SM, Vodyanoy I (1997) Stochastic resonance in non-dynamical systems without response thresholds. *Nature* 385:319–321.

Bulsara A, Jacobs EW, Zhou T, Moss F, Kiss L (1991) Stochastic resonance in a single neuron model: Theory and analog simulation. *J. Theor. Biol.* 152:531–555.

Capurro A, Pakdaman K, Nomura T, Sato S (1998) Aperiodic stochastic resonance with correlated noise. *Phys. Rev. E* 58:4820–4827.

Chialvo DR, Apkarian AV (1993) Modulated noisy biological dynamics: Three examples. *J. Stat. Phys.* 70:375–391.

Chow CC, Imhoff TT, Collins JJ (1998) Enhancing aperiodic stochastic resonance through noise modulation. *Chaos* 8:616–620.

Collins JJ, Chow CC, Imhoff TT (1995) Stochastic resonance without tuning. *Nature* 376:236–238.

Collins JJ, Imhoff TT, Grigg P (1996) Noise enhanced information transmission in rat SA1 cutaneous mechanoreceptors via aperiodic stochastic resonance. *J. Neurophysiol.* 76:642–645.

Contreras D, Destexhe A, Steriade M (1997) Intracellular and computational characterization of the intracortical inhibitory control of synchronized thalamic inputs in vivo. *J. Neurophysiol.* 78:335–350.

Contreras D, Timofeev I, Steriade M (1996) Mechanisms of long lasting hyperpolarizations underlying slow sleep oscillations in cat corticothalamic networks. *J. Physiol.* 494:251–264.

Cook EP, Johnston D (1997) Active dendrites reduce location-dependent variability of synaptic input trains. *J. Neurophysiol.* 78:2116–2128.

Cragg BG (1967) The density of synapses and neurons in the motor and visual areas of the cerebral cortex. *J. Anat.* 101:639–654.

DeFelipe J, Fariñas I (1992) The pyramidal neuron of the cerebral cortex: Morphological and chemical characteristics of the synaptic inputs. *Prog. Neurobiol.* 39:563–607.

Denk W, Webb WW (1989) Thermal-noise-limited transduction observed in mechanosensory receptors of the inner ear. *Phys. Rev. Lett.* 63:207–210.

Destexhe A, Mainen ZF, Sejnowski TJ (1998) Kinetic models of synaptic transmission. In: Koch C, Segev I, eds. *Methods in Neuronal Modeling* (2nd ed.). MIT Press, Cambridge, MA, pp. 1–26.

Destexhe A (2001) Simplified models of neocortical pyramidal cells preserving somatodendritic voltage attenuation. *Neurocomputing*. 38:167–173.

Destexhe A, Paré D (1999) Impact of network activity on the integrative properties of neocortical pyramidal neurons in vivo. *J. Neurophysiol.* 81:1531–1547.

Douglas RJ, Wilkens L, Pantazelou E, Moss F (1993) Noise enhancement of information transfer in crayfish mechanoreceptors by stochastic resonance. *Nature* 365:337–340.

Evarts EV (1964) Temporal patterns of discharge of pyramidal tract neurons during sleep and waking in the monkey. *J. Neurophysiol.* 27:152–171.

Fauve S, Heslot FJ (1993) Stochastic resonance in a bistable system. *Phys. Lett.* A97:5–7.

French CR, Sah P, Buckett KJ, Gage PW (1990) A voltage-dependent persistent sodium current in mammalian hippocampal neurons. *J. Gen. Physiol.* 95:1139–1157.

Gammaitoni L, Hänggi P, Jung P, Marchesoni F (1998) Stochastic resonance. *Rev. Mod. Phys.* 70:223–287.

Gerstein GL, Bedenbaugh P, Aertsen AJ (1989) Neuronal assemblies. *IEEE Trans. Biomed. Eng.* 36:4–14.

Gruner JE, Hirsch JC, Sotelo C (1974) Ultrastructural features of the isolated suprasylvian gyrus. *J. Comp. Neurol.* 154:1–27.

Hines ML, Carnevale NT (1997) The NEURON simulation environment. *Neural Computation* 9:1179–1209.

Hô N, Destexhe A (2000) Synaptic background activity enhances the responsiveness of neocortical pyramidal neurons. *J. Neurophysiol.* 84:1488–1496.

Hodgkin AL, Huxley AF (1952) A quantitative description of membrane current and its application to conduction and excitation in nerve. *J. Physiol.* 117:500–544.

Hubel D (1959) Single-unit activity in striate cortex of unrestrained cats. *J. Physiol.* 147:226–238.

Huber MT, Krieg JC, Dewald M, Voigt K, Braun HA (1998) Stimulus sensitivity and neuromodulatory properties of noise intrinsic neuronal oscillators. *BioSystems* 48:95–104.

Huguenard JR, Hamill OP, Prince DA (1988) Developmental changes in Na^+ conductances in rat neocortical neurons: Appearance of a slow inactivating component. *J. Neurophysiol.* 59:778–795.

Huguenard JR, McCormick DA (1992) Simulation of the currents involved in rhythmic oscillations in thalamic relay neurons. *J. Neurophysiol.* 68:1373–1383.

Ivey C, Apkarian AV, Chivalvo DR (1998) Noise-induced tuning curve changes in mechanoreceptors. *J. Neurophysiol.* 79:1879–1890.

Jaramillo F, Wiesenfeld K (1998) Mechanoelectrical transduction assisted by Brownian motion: A role for noise in the auditory system. *Nature Neuroscience* 1:384–388.

Johnston D, Magee JC, Colbert CM, Cristie BR (1996) Active properties of neuronal dendrites. *Annual Rev. Neurosci.* 19:165–186.

Lampl I, Reichova I, Ferster D (1999) Synchronous membrane potential fluctuations in neurons of the cat visual cortex. *Neuron* 22:361–374.

Larkman AU (1991) Dendritic morphology of pyramidal neurons of the visual cortex of the rat. III. Spine distributions. *J. Comp. Neurol.* 306:332–343.

Lee SG, Kim S (1999) Parameter dependence of stochastic resonance in the stochastic Hodgkin-Huxley neuron. *Phys. Rev. E* 60:826–830.

Lee SG, Neiman A, Kim S (1998) Coherence resonance in a Hodgkin-Huxley neuron. *Phys. Rev. E* 57:3292–3297.

Levin JE, Miller JP (1996) Broadband neural coding in the cricket sensory system enhanced by stochastic resonance. *Nature* 380:165–168.

Longtin A (1993) Stochastic resonance in neuron models. *J. Stat. Phys.* 70:309–327.

Longtin A, Bulsara A, Moss F (1991) Time-interval sequences in bistable systems and the noise-induced transmission of information by sensory neurons. *Phys. Rev. Lett.* 67:656–659.

Longtin A, Chialvo DR (1998) Stochastic and deterministic resonance for excitable systems. *Phys. Rev. Lett.* 81:4012–4015.

Lytton WW (1996) Optimizing synaptic conductance calculation for network simulations. *Neural Computation* 8:501–509.

Magee JC, Johnston D (1995a) Characterization of single voltage-gated sodium and calcium channels in the apical dendrites of rat CA1 pyramidal neurons. *J. Physiol.* 487:67–90.

Magee JC, Johnston D (1995b) Synaptic activation of voltage-gated channels in the dendrites of hippocampal pyramidal neurons. *Science* 268:301–304.

Mar DJ, Chow CC, Gerstner W, Adams RW, Collins JJ (1999) Noise shaping in populations of coupled model neurons. *Proc. Natl. Acad. Sci. USA* 96:10450–10455.

Mato G (1998) Stochastic resonance in neural systems: Effects of temporal correlation in the spike trains. *Phys. Rev. E* 58:876–880.

Matsumura M, Cope T, Fetz EE (1988) Sustained excitatory synaptic input to motor cortex neurons in awake animals revealed by intracellular recording of membrane potentials. *Exp. Brain Res.* 70:463–469.

McCormick DA, Huguenard JR (1992) A model of the electrophysiological properties of thalamocortical relay neurons. *J. Neurophysiol.* 68:1384–1400.

Migliore M, Hoffman DA, Magee JC, Johnston D (1999) Role of an A-type K^+ conductance in the back-propagation of action potentials in the dendrites of hippocampal pyramidal neurons. *J. Comp. Neurosci.* 7:5–15.

Neiman A, Pei X, Russell D, Wojtenek W, Wilkens L, Moss F, Braun HA, Huber MT, Voigt K (1999a) Synchronization of the noisy electrosensitive cells in the paddlefish. *Phys. Rev. Lett.* 82:660–663.

Neiman A, Schimansky-Geier L, Moss F, Shulgin B, Collins JJ (1999b) Synchronization of noisy systems by stochastic signals. *Phys. Rev. E* 60:284–292.

Nicolis C (1982) Stochastic aspects of climatic transitions: Response to a periodic forcing. *Tellus* 34:1.

Nowak LG, Sanchez-Vives MV, McCormick DA (1997) Influence of low and high frequency inputs on spike timing in visual cortical neurons. *Cereb. Cortex* 7:487–501.

Paré D, Shink E, Gaudreau H, Destexhe A, Lang EJ (1998) Impact of spontaneous synaptic activity on the resting properties of cat neocortical neurons in vivo. *J. Neurophysiol.* 79:1450–1460.

Pei X, Wilkens AL, Moss F (1996) Light enhances hydrodynamic signaling in the multimodal caudal photoreceptor interneurons of the crayfish. *J. Neurophysiol.* 76:3002–3011.

Press WH, Teukolsky SA, Vetterling WT, Flannery BP (1993) *Numerical Recipes in C: The Art of Scientific Computing*. (2nd ed.). Cambridge University Press, Cambridge.

Richardson KA, Imhoff TT, Grigg P, Collins JJ (1998) Using electrical noise to enhance the ability of humans to detect subthreshold mechanical cutaneous stimuli. *Chaos* 8:599–603.

Rudolph M, Destexhe A (2000) Models of neocortical pyramidal neurons in the presence of correlated synaptic background activity: High discharge variability, enhanced responsiveness and independence of input location. *Soc. Neurosci. Abstracts* 26:1623.

Segev I, Rall W (1998) Excitable dendrites and spines: Earlier theoretical insights elucidate recent direct observations. *Trends Neurosci.* 21:453–460.

Shimokawa T, Rogel A, Pakdaman K, Sato S (1999) Stochastic resonance and spike-timing precision in an ensemble of leaky integrate and fire neuron models. *Phys. Rev. E* 59:3461–3470.

Simonotto E, Riani M, Seife C, Roberts M, Twitty J, Moss F (1997) Visual perception of stochastic resonance. *Phys. Rev. Lett.* 78:1186–1189.

Srebo R, Malladi P (1999) Stochastic resonance of the visually evoked potential. *Phys. Rev. E* 59:2566–2570.

Stacey WC, Durand DM (2000) Stochastic resonance improves signal detection in hippocampal CA1 neurons. *J. Neurophysiol.* 83:1394–1402.

Steriade M (1978) Cortical long-axoned cells and putative interneurons during the sleep-waking cycle. *Behav. Brain Sci.* 3:465–514.

Steriade M, Timofeev I, Grenier F (2001) Natural waking and sleep states: A view from inside neocortical neurons. *J. Neurophysiol.* 85:1969–1985.

Stuart GJ, Sakmann B (1994) Active propagation of somatic action potentials into neocortical pyramidal cell dendrites. *Nature* 367:69–72.

Szentagothai J (1965) The use of degeneration in the investigation of short neuronal connections. In: Singer M, Shade JP, eds. *Progress in Brain Research* 14. Elsevier, Amsterdam. pp. 1–32.

Traub RD, Miles R (1991) *Neuronal Networks of the Hippocampus*. Cambridge University Press, Cambridge.

Wang W, Wang Y, Wang ZD (1998) Firing and signal transduction associated with an intrinsic oscillation in neuronal systems. *Phys. Rev. E* 57:R2527–R2530.

White EL (1989) *Cortical Circuits*. Birkhauser, Boston.

Wiesenfeld K, Moss F (1995) Stochastic resonance and the benefits of noise: From ice ages to crayfish and SQUIDS. *Nature* 373:33–36.

Yamada WM, Koch C, Adams PR (1989) Multiple channels and calcium dynamics. In: Koch C, Segev I, eds. *Methods in Neuronal Modeling*. MIT Press, Cambridge, MA.

Zhou T, Moss F (1990) Analog simulations of stochastic resonance. *Phys. Rev.* A41:4255–4264.

Zohary E, Shadlen MN, Newsome WT (1994) Correlated neuronal discharge rate and its implications for psychophysical performance. *Nature* 370:140–143.